NASA TECHNICAL NOTE

NASA TN D-3858

NASA TN D-3858

EXPERIMENTAL INVESTIGATION OF THE TURBULENT BOUNDARY LAYER AT A MACH NUMBER OF 6 WITH HEAT TRANSFER AT HIGH REYNOLDS NUMBERS

by Richard D. Samuels, John B. Peterson, Jr., and Jerry B. Adcock

Langley Research Center
Langley Station, Hampton, Va.

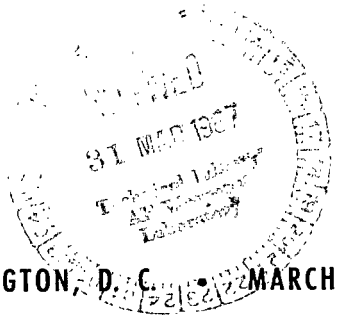

NATIONAL AERONAUTICS AND SPACE ADMINISTRATION • WASHINGTON, D. C. • MARCH 1967

EXPERIMENTAL INVESTIGATION OF THE TURBULENT BOUNDARY LAYER AT A MACH NUMBER OF 6 WITH HEAT TRANSFER AT HIGH REYNOLDS NUMBERS

By Richard D. Samuels, John B. Peterson, Jr.,
and Jerry B. Adcock

Langley Research Center
Langley Station, Hampton, Va.

NATIONAL AERONAUTICS AND SPACE ADMINISTRATION

For sale by the Clearinghouse for Federal Scientific and Technical Information
Springfield, Virginia 22151 – CFSTI price $3.00

EXPERIMENTAL INVESTIGATION OF THE TURBULENT BOUNDARY LAYER AT A MACH NUMBER OF 6 WITH HEAT TRANSFER AT HIGH REYNOLDS NUMBERS

By Richard D. Samuels, John B. Peterson, Jr.,
and Jerry B. Adcock
Langley Research Center

SUMMARY

An experimental investigation of turbulent boundary-layer skin friction and heat transfer on a hollow cylinder was made at a Mach number of 6 and with two wall temperatures at Reynolds numbers based on distance from the virtual origin from 2.4×10^6 to 28.7×10^6. Data obtained include total-temperature profiles, velocity profiles, average skin-friction coefficients obtained by the momentum method, and Stanton numbers obtained from use of heat flowmeters.

The measured temperatures in the boundary layer were compared with two theoretical distributions, the Crocco laminar distribution used by Van Driest (NACA TN 2597) and a quadratic distribution used by Donaldson (NACA RM L52H04). The skin-friction coefficients were compared with the theories of Van Driest, Monaghan and Johnson, Sommer and Short, and Spalding and Chi. Stanton numbers were also compared with these theories in conjunction with the Colburn modification of Reynolds analogy.

Experimental results indicate that at high Reynolds numbers wall-temperature ratio has no appreciable effect on the average skin-friction coefficient. At high Reynolds numbers, the theory of Spalding and Chi gave fair agreement with the experimental data. However, the Colburn modification of Reynolds analogy along with the turbulent skin-friction theory of Spalding and Chi underestimates the measured heat-transfer coefficient.

INTRODUCTION

Recently, serious consideration has been given to the design and construction of a hypersonic cruise aircraft. The level of skin friction is very important in the design of such an aircraft since skin friction will constitute a large portion of the total drag. However, the extent of the variations between the various theories for predicting the hypersonic turbulent boundary-layer skin friction make it difficult to estimate the performance of hypersonic aircraft.

Experimental values for hypersonic turbulent skin friction taken at zero heat transfer show a considerable amount of scatter. (See ref. 1.) There is also uncertainty in the effect of wall-temperature ratio on hypersonic turbulent skin friction. For instance, Winkler and Cha in reference 2 and Danberg in reference 3 report that hypersonic turbulent skin friction decreases with a decrease in wall-temperature ratio, whereas Sommer and Short in reference 4 report the opposite trend.

Accurate heat-transfer information for hypersonic cruise aircraft is also necessary to obtain an efficient structural design. Generally, some form of Reynolds analogy is used to predict turbulent boundary-layer heat transfer from the theories for turbulent skin friction. There are several theories for the value of the Reynolds analogy factor in a turbulent boundary layer. These theories attempt to account for the effects on the Reynolds analogy factor of compressibility and of changes in Prandtl number in the turbulent boundary layer.

The purpose of this investigation was to obtain experimental information on the skin friction and heat transfer in a hypersonic turbulent boundary layer at high Reynolds numbers and with a zero pressure gradient in order to help determine the theories which most accurately predict compressible turbulent skin friction and heat transfer. Heat-transfer and skin-friction coefficients were obtained on a hollow cylinder at Mach 6 and at two wall-temperature ratios, 0.44 and 0.50. This report is an extension of previous results obtained at zero heat transfer and reported in reference 1. The Reynolds number range of the investigation was from 2.4 to 28.7×10^6. Turbulent boundary-layer velocity profiles were obtained from pitot-pressure and total-temperature surveys on the hollow cylinder. The boundary-layer momentum thickness was obtained from the survey data, and average skin-friction coefficients were determined from the boundary-layer momentum thicknesses.

Heat fluxes were determined at several stations by the use of heat flowmeters. Measured surface wall-temperature distribution along with the heat flux and the adiabatic wall temperature were used to calculate the heat-transfer coefficients and the Stanton numbers.

The present skin-friction coefficients, along with other experimental skin-friction data, are compared with four well-known theories of turbulent boundary-layer skin friction with heat transfer; Sommer and Short (ref. 4), Monaghan and Johnson (ref. 5), Van Driest (ref. 6), and Spalding and Chi (ref. 7). A comparison is also made between these four theories and the experimentally measured heat-transfer coefficients by using the generally accepted Colburn modification of Reynolds analogy (ref. 8) to convert the skin-friction theories to heat-transfer theories.

SYMBOLS

A, B, C a, b, c, d K	constants
C_F	average skin-friction coefficient
C_f	local skin-friction coefficient
c_p	specific heat at constant pressure
h	heat-transfer coefficient
M	Mach number
N_{Pr}	Prandtl number
N_{St}	Stanton number
p	pressure
p'	pitot pressure
q	heat flux
R_{le}	Reynolds number based on distance from leading edge
R_{le-x}	Reynolds number based on distance from leading edge to virtual origin of turbulent boundary layer
R_x	Reynolds number based on distance from virtual origin of turbulent boundary layer
R_θ	Reynolds number based on momentum thickness
S	surface area
r	radius of cylinder

T	temperature
u	velocity
x	distance from virtual origin of turbulent boundary layer
x_{le}	distance from leading edge of model
y	distance, or height, normal to model and measured from surface
δ	boundary-layer thickness
δ_p	boundary-layer thickness based on pitot-pressure survey
η_p	probe recovery factor, $\eta_p = \frac{T_p - T}{T_t - T}$
θ	momentum thickness of boundary layer
θ^I, θ^{II}	coefficients used in eq. (2)
ρ	gas density

Subscripts:

aw	adiabatic wall
i	incompressible
p	measured by boundary-layer probe
t	total or stagnation conditions
w	wall or wall conditions
δ	conditions at edge of boundary layer

APPARATUS

Wind Tunnel

The tests were conducted in the Langley 20-inch Mach 6 tunnel. Although the tunnel is of the blowdown variety, the air supply pumps are of sufficient capacity to make possible runs of a 45-minute duration. The rectangular test section of the tunnel measures 20.0 inches (50.8 cm) by 20.5 inches (52.1 cm). The maximum possible stagnation temperature is about 1060° R (590° K) and the maximum stagnation pressure attainable is about 525 psia (3.62 MN/m^2). Further details and a schematic drawing of the tunnel can be found in reference 9.

Model

A schematic drawing of the hollow cylinder model used in this test is shown in figure 1. The outside diameter of the model is 6 inches (15 cm) for the first 42 inches (107 cm). The model then flares at a 20° angle to an outside diameter of 8 inches (20 cm). The model was flared in order to facilitate the cooling of the model which was accomplished by circulating a liquid freon coolant through the hollow walls of the cylinder. The overall length of the model was 48 inches (122 cm). The leading edge was beveled at a 15° angle to an inside diameter of 5 inches (13 cm).

To promote turbulent flow, a boundary-layer trip was located at 1.15 inches (2.92 cm) from the leading edge. The trip consisted of 0.075-inch (0.190-cm) diameter steel rods mounted perpendicular to the surface at 0.25-inch (0.63-cm) intervals on the perimeter of the model. The rods were ground to a height of 0.025 inch (0.063 cm). Further information concerning the boundary-layer trip can be found in reference 1.

Cooling Equipment

The liquid freon coolant was circulated through the model by using a centrifugal pump with a maximum flow of 50 gal per min (0.003 m^3/sec). The pump was driven by a 15 hp (11.2 kW) electric motor. A diagram of the cooling system is shown in figure 2. The freon was cooled to temperatures several degrees below the desired model temperatures (360° R and 340° R (200° K and 189° K)). The cooling was accomplished by bubbling liquid nitrogen through the freon in the storage tank. The relation of the temperatures of the coolant could also be controlled by bypassing a portion of the coolant as it returned from the model and recirculating this portion directly to the model rather than returning it to the cooling tank. In this way the model wall temperature could be controlled adequately for the duration of a run.

Model Instrumentation

Static pressure orifices were located on the top, bottom, and sides of each model at three positions: 18, 26, and 34 inches (46, 66, and 88 cm) from the leading edge. Another orifice was located on the top of the model, 10 inches (25 cm) from the leading edge. The static pressures were measured with a 0 to 1 psia (0 to 6.89 kN/m^2) Statham pressure transducer, which has an accuracy of within 1 percent of full scale, mounted on an electrically actuated scanning valve. Therefore all the static orifices were read by the same transducer, thus, a more accurate comparison was made between static pressures at various positions on the model. A zero reading was taken on all pressure transducers before each run by using a reference pressure of 0.25 psia (1.72 kN/m^2). This reference pressure was determined by use of a Wallace and Tiernan 0 to 100 mm Hg dial gage.

The wall temperatures were measured during each run by use of five swaged, copper-constantan thermocouples welded to the inside surface of the 0.120-inch (0.305-cm) thick outside wall at distances of 6, 14, 22, 30, and 38 inches (15, 35, 56, 76, and 96 cm) from the leading edge. The thermocouples were referenced to an insulated junction box outside the tunnel. A 12-channel recording potentiometer was used to read the temperature of the junction box.

The heat transfer was measured by use of heat flowmeters placed in the outside shell of the model at 12, 24, and 36 inches (31, 61, and 94 cm) from the leading edge. The design for a differential thermocouple heat flowmeter as described in reference 10 was adapted to the model. The heat flowmeter shown in cross-sectional view in figure 3 consisted of a disk, made of an alloy of 55 percent copper and 45 percent nickel, sandwiched between two layers of stainless steel. The output voltage of each of the heat flowmeters was amplified before being recorded. The amplification factor for heat flowmeters 1 and 2 was 50, and the amplification factor for heat flowmeter 3 was 100. The amplified heat flowmeter output and the associated model inner-surface thermocouple outputs were recorded on a digital tape system during the tunnel run. The heat flowmeters used in this test were calibrated by using a radiant heat source. The same dc amplifiers that were used during the test were used during the calibration. In order to be assured that the gages would have the same thermal properties during the calibration as during the test, liquid freon at approximately 360° R (200° K) was used to cool the heat flowmeters during the calibration. It should be noted that a flange conduction correction, as applied in reference 10, was not necessary for this investigation because of the nature of the calibration. During the calibration the same flange conduction was present as during the tests.

Calibrations of the heat flowmeters at 340° R (188° K) showed no change in the original calibration. During calibration, the amplifier output was compared with the

radiant heat flux as determined by the output from a standard calorimeter. The final calibration curves for each heat meter and amplifier combination are shown in figure 4.

Probes and Boundary-Layer Survey Apparatus

Schematic drawings of the total-pressure and total-temperature probes are shown in figures 5 and 6, respectively.

The pressure probe was made of 0.050-inch (0.127-cm) outside diameter stainless-steel tubing flattened to a height of 0.007 inch (0.018 cm) with an opening height of 0.003 inch (0.008 cm) at the tip. The tube was silver soldered into progressively larger tubing which led to the 0.25-inch (0.42-cm) outside diameter tubing of which the vertical shaft was formed.

The boundary-layer survey pitot pressure was measured by three Statham pressure transducers, which have an accuracy of within 1 percent of full scale, manifolded together and connected to another electrically actuated scanning valve. The ranges of the three transducers were 0 to 1 psia (0 to 6.9 kN/m^2), 0 to 5 psia (0 to 34.5 kN/m^2), and 0 to 15 psia (0 to 103 kN/m^2). A zero reading was taken on all pressure transducers before each run by using a reference pressure of 0.25 psia (1.72 kN/m^2). This reference pressure was determined by a Wallace and Tiernan 0 to 100 mm Hg dial gage.

The temperature probe shown in figure 6 was made from an 0.014-inch (0.036-cm) outside diameter swaged thermocouple. Two 0.007-inch (0.018-cm) diameter holes were drilled in the side wall for exits. The thermocouple wires were 0.001-inch (0.0025-cm) diameter chromel-alumel wires. The reference junction was placed in an ice bath outside the tunnel.

The temperature probe was calibrated at 610° R (339° K) in the Langley Unitary Plan wind tunnel. Figure 7 shows the variation of probe recovery factor with Mach number and unit Reynolds number.

The probe survey mechanism was driven by an electric motor and could position the probe in boundary layer within an accuracy of 0.002 inch (0.005 cm) over a range of 1 inch (2.54 cm). A further discussion of the apparatus can be found in reference 1.

Tests

The tests were conducted at a free-stream Mach number of 6. The tunnel stagnation pressure was approximately 525 psia (3.62 MN/m^2). The tests were run at the two previously mentioned wall-temperature ratios $\left(\frac{T_w}{T_{aw}} = 0.50 \text{ and } \frac{T_w}{T_{aw}} = 0.44\right)$. These ratios were obtained by using two stagnation temperatures which were approximately 872° R (485° K) and 975° R (542° K) and two model wall temperatures which were

approximately 390° R (217° K) and 380° R (211° K). The respective ratios of wall temperature to free-stream total temperature were approximately 0.45 and 0.39. The Reynolds numbers per foot were approximately 9.94×10^6 (32.6×10^6 per meter) and 8.72×10^6 (28.6×10^6 per meter), respectively. Total-temperature and total-pressure surveys of the boundary layer were made at five stations. These stations were on top of the model at 8, 11, 33, 37, and 40 inches (20, 28, 84, 94, and 102 cm), which will be referred to as stations 1 to 5 throughout this report. Schlieren photographs were also taken to study boundary-layer transition and were similar to those shown in reference 1.

RESULTS AND DISCUSSION

Wall-Temperature Distribution

As mentioned earlier, the wall temperature was measured at five stations along the model by thermocouples welded to the inside of the 0.120-inch (0.305-cm) thick stainless-steel outer wall. By knowing the heat flux through the wall, the thickness of the wall, and the thermal conductivity of 304 stainless steel, the temperature difference across the wall was calculated. This temperature difference, which amounted to less than $15\ R^{\circ}$ ($8\ K^{\circ}$), was added to the measured wall temperature. Figure 8 shows T_w/T_t as a function of the distance from the leading edge for each wall-temperature ratio. The wall temperature is seen to be virtually independent of distance from the leading edge. Also shown is T_w/T_t as determined in the adiabatic tests (ref. 1).

Pressure Surveys

Boundary-layer pitot-pressure surveys, presented in table 1, were made at the five stations previously mentioned. One of these surveys is shown in figure 9. The thickness of the boundary layer δ_p was determined for each run from data such as that shown in figure 9. The thickness δ_p was taken to be the point of intersection between the vertical line, which represents the free-stream value of pitot pressure, and the line through the last few data points taken just inside the boundary layer. The values of δ_p were found in the same manner as in reference 1. The values of δ_p for each station are shown in table 2. From the pitot-pressure surveys and the assumption of constant static pressure, the nondimensional Mach number profiles shown in figure 10 were obtained. At a given nondimensional height y/δ_p in the boundary layer, the Mach number decreases with increasing distance from the leading edge to station 3; the three rearward stations are virtually the same.

Temperature Surveys

The temperature surveys presented in table 3 were made with a probe only slightly different in design from that described in reference 1. However, both probes were calibrated in the Langley Unitary Plan wind tunnel at the same time. For the present investigation, surveys were made at 5 stations for the highest heat-transfer rate and at only the three rearward stations for the lowest heat-transfer rate. By using the Mach number and temperature-survey data, the total-temperature profile can be obtained by the following iterative procedure. The probe recovery factor η_p is assumed, the corresponding total temperature and Reynolds number calculated, and a new η_p determined. This procedure is repeated until the assumed η_p agrees with the calculated value.

The total-temperature profiles for each heat-transfer rate are shown in figure 11. Plotted as the ordinate is y/δ_p where y is the distance from the surface and δ_p is the boundary-layer pitot-pressure thickness. By comparing figures 11(a) and 11(b), it can be seen that the three rearward station profiles are similar for each of the heat-transfer ratios. Also obvious from figure 11 is the existence of a temperature "bump." This bump, where the boundary-layer total temperature exceeds the free-stream total temperature, has a magnitude of approximately 2.5 percent of the free-stream total temperature. The temperature bumps for these nonadiabatic cases are higher than those for the adiabatic case in reference 1 and are inconsistent with expected trends.

Figure 12 shows the boundary-layer total temperature as a function of the velocity ratio squared for each station at each heat-transfer rate. Two theoretical profiles are also shown. The quadratic profile, found in reference 11, is similar to the Crocco quadratic form. In terms of total-temperature ratio, the equation is of the form

$$\frac{T_t}{T_{t,\delta}} = A\left(\frac{u}{u_\delta}\right)^2 + B\frac{u}{u_\delta} + C \tag{1}$$

where

$$A = 1 - \frac{T_{aw}}{T_{t,\delta}}$$

$$B = \frac{T_{aw}}{T_{t,\delta}} - \frac{T_w}{T_{t,\delta}}$$

and

$$C = \frac{T_w}{T_{t,\delta}}$$

As can be seen, the quadratic form predicts higher values than were measured through the inner and middle portion of the boundary layer. However, the quadratic fails to predict the temperature bump. In order to determine if a temperature bump might be expected at the wall-temperature ratios of this investigation, Crocco's laminar theory, as presented in reference 12, was computed and plotted in figure 12. In the nomenclature of the present report, Crocco's laminar theory is expressed by

$$\frac{T_t}{T_{t,\delta}} = \frac{T_w}{T_{t,\delta}} - \left(\frac{T_w}{T_{t,\delta}} - \frac{T_\delta}{T_{t,\delta}}\theta^I\right) + \left(1 - \frac{T_\delta}{T_{t,\delta}}\right)\left[2\theta^{II} + \left(\frac{u}{u_\delta}\right)^2\right] \tag{2}$$

where θ^I and θ^{II} are constants depending only on Prandtl number and velocity ratio. For this investigation the Prandtl number was assumed to be 0.725. The laminar distribution, in fact, predicts a bump in the outer portion of the boundary layer at the wall-temperature ratios of this investigation, although it is of smaller magnitude than obtained in the present investigation. The bump predicted by Crocco's laminar theory decreases with heat transfer, as expected. (See fig. 12, and fig. 10 of ref. 1.)

Velocity Profiles

The boundary-layer velocity profiles, as shown in figure 13, were calculated by using the measured total temperature and the Mach number distribution as determined directly from the boundary-layer pressure surveys.

Since no total-temperature surveys were made at stations 1 and 2 for the higher wall-temperature ratio, it was necessary to use an assumed profile. In view of the fact that the profiles for both wall-temperature ratios were similar at stations 3, 4, and 5, the assumed profiles at stations 1 and 2 were made similar to the profiles at stations 1 and 2 for the lower wall-temperature ratio.

The profiles yielded velocity ratios which were greater than unity. In an attempt to explain this velocity overshoot, the Mach number distribution was studied. The Mach number distribution was obtained by assuming that the static pressure was constant through the boundary layer and by using the measured total pressure. As much as a 15 percent change in the static pressure through the boundary layer would be necessary to account for these velocity overshoots if the sole effect is a change in static pressure. Measurements of the static pressure at the wall and just outside the boundary layer by Lobb, Winkler, and Persh at hypersonic Mach numbers in a tunnel wall boundary layer (ref. 13) show a change of 1 percent or less.

The total-temperature profiles were considered next. The bump discussed earlier is to be expected for adiabatic wall flow; however, the magnitude of the bump found in the present cooled wall tests was not expected. As discussed earlier, the temperature probe was calibrated in the free stream of the Langley Unitary Plan wind tunnel. Under these

conditions the flow on the probe shield was probably laminar. Therefore, when the probe was used in the turbulent boundary layer, turbulence on the shield might affect the probe recovery factor. This effect would be expected to be greatest in the outer parts of the boundary layer since the maximum turbulent intensity of a hypersonic turbulent boundary layer is found in the outer parts.

To avoid any velocity overshoot in the boundary layer by using the measured temperature probe profile, it is of interest to note that it would have been necessary that the temperature probe recovery factor η_p be higher in the boundary layer where the Reynolds number was lower than it was in the free stream where the Reynolds number was higher. (The boundary-layer pitot-pressure measurements were assumed to be correct.) This trend is opposite that indicated by the probe calibration, which shows that the temperature probe recovery factor η_p decreases as the Reynolds number decreases. However, η_p might have been increased by the turbulence in the boundary layer since turbulent flow on the temperature probe shield would increase the recovery factor on the outside of the shield.

This 1 percent velocity overshoot was greatly magnified in the value of momentum thickness as calculated from

$$\theta = \int_0^{\delta} \frac{\rho u}{\rho_\delta u_\delta} \left(1 - \frac{u}{u_\delta}\right)\left(\frac{r + y}{r}\right) dy \tag{3}$$

It is believed that any errors in the temperature probe measurements in the interior of the boundary layer were smaller than those in the outer parts since the turbulence level is lower in the interior of the boundary layer. Therefore, the velocities calculated in the interior of the boundary layer were believed to be more accurate. In order to fair the velocity profiles to the free-stream velocity at the edge of the boundary layer, the velocities through the middle of the boundary layer were fitted to an exponential curve:

$$\frac{u}{u_\delta} = 1 - ae^{-K\left(\frac{y}{\delta_p} - \frac{b}{\delta_p}\right)^2} \tag{4}$$

The arbitrary constants a, b, and K were determined for each run. The velocities at the points near the outer edge of the boundary layer were obtained from the exponential curve. The difference in the measured values and exponentially calculated values is shown in figure 14 where the exponential values are represented by dashed lines. Figure 15 illustrates the difference in momentum defect profile obtained by using the measured values and the exponentially calculated values. (In this figure also the dashed line represents the exponential values.) It should be noted that the effect of small changes in

u/u_δ on the momentum defect is greater in the outer parts of the boundary layer than in the interior of the boundary layer. Therefore the accuracy of the momentum defect profile should be greater in the interior of the boundary layer than the accuracy indicated in figure 15 for the outer portions of the boundary layer.

Longitudinal Mach Number Distribution

The longitudinal Mach number distribution as determined both from the ratio of the free-stream static pressure to free-stream total pressure and from the ratio of the free-stream pitot pressure to free-stream total pressure is shown in figure 16. The slight Mach number gradient can be compensated for by the method used by Wilson in reference 14 to account for the lack of constant flow conditions along the edge of the boundary layer. However, this correction was considered to be insignificant for the present investigation.

Virtual Origin

All theories are based on the assumption that a fully turbulent boundary layer exists from the leading edge. As is well known, in reality there is a laminar portion, transitional portion, and then a fully turbulent portion. In order to compare experimental data with other data or with theory, it is necessary to base Reynolds number on an effective length. The effective length for this investigation is based on the distance from the virtual origin to the particular measuring station. The virtual origin is the point at which a fully turbulent boundary layer of equivalent thickness to that of the experimental boundary layer would have necessarily originated. The location of the virtual origin was determined by the method of least squares given in reference 15. The momentum thickness is assumed to grow according to the relation

$$R_\theta = c\left(R_{le} - R_{le\text{-}x}\right)^d \tag{5}$$

where c, d, and $R_{le\text{-}x}$ are unknown and determined from the experimental data. The least squares method gives the values for the constants which most accurately match the experimental data.

Determination of Skin Friction and Comparison With Theory and Other Experiments

The skin-friction results were obtained by plotting Reynolds number based on momentum thickness against length Reynolds number. Figure 17 shows R_θ as a function of both the Reynolds number based on distance from the leading edge and the

Reynolds number based on distance from the virtual origin. The average skin friction was found from the equation

$$C_F = \frac{2R_\theta}{R_x} \tag{6}$$

where R_θ is based on the value of θ obtained from the exponential form.

Shown in figure 18 is the variation of average skin friction with effective Reynolds numbers for each heat-transfer rate. Also shown are the values predicted by the four theories. At both heat-transfer rates, the present data seem to be in fair agreement with Spalding and Chi at the higher Reynolds numbers. It is believed that at the lower Reynolds numbers the skin friction is somewhat in error for two reasons. First, C_F is sensitive to the location of virtual origin for the forward stations. Second, any error in momentum thickness which might be present is more pronounced for the thinner boundary layer at the first two stations than for the rearward stations.

Figure 19 shows the variation of the ratio of average skin friction to incompressible skin friction with Reynolds number for various wall-temperature ratios. The points shown at adiabatic wall temperature $\left(T_w/T_{aw} = 1\right)$ are the data presented in reference 1 using the least squares method for a virtual origin. Figure 20, which is a cross plot of the data in figure 19, shows the variation of the ratio of average skin friction to incompressible skin friction, at various Reynolds numbers, with wall-temperature ratio. As can be seen, there is no appreciable change in the ratio of skin friction to wall temperature at any of the higher Reynolds numbers. This trend is unexpected since data at lower Mach numbers show that skin friction generally increased with a decrease in wall temperature. (See ref. 4.)

Figure 21 is a three-dimensional plot comparing various experimental results (refs. 1 to 4, 14, and 16 to 22) with the present results. The surface shown represents the variation of the average skin-friction ratio $C_F/C_{F,i}$ with Mach number and wall-temperature ratio as predicted by Sommer and Short for an effective Reynolds number of 10×10^6. The open symbols represent data obtained at Reynolds numbers less than or equal to 10×10^6, and the solid symbols represent data at higher Reynolds numbers. In general, the present data show the same trend as the other experimental data, especially for Mach numbers greater than 5. The skin friction decreases with increasing Reynolds number but, in general, remains higher than predicted by Sommer and Short. The present data for Reynolds numbers greater than 19×10^6 fall below the value predicted by Sommer and Short in the same manner as data for other high Reynolds numbers.

Heat Transfer

Figure 22 shows the variation of Stanton number with Reynolds number. The Stanton number was obtained from the equation

$$N_{St} = \frac{h}{\rho_\delta u_\delta c_p} \tag{7}$$

where

$$h = \frac{q/S}{T_{aw} - T_w} \tag{8}$$

The theories shown are skin-friction theories which have been transformed by use of the Colburn analogy where $2N_{St}/C_f = N_{Pr}^{-2/3}$. A Prandtl number of 0.725 was assumed. The present data indicate that the Stanton number does not decrease as rapidly with Reynolds number as these theories predict.

Figure 23 indicates the variation of Stanton number with Reynolds number based on momentum thickness. The Stanton number from the present data tends to decrease slightly with momentum thickness Reynolds number. This trend is the same as reported in references 2, 3, and 23.

Figure 24 is a three-dimensional plot of heat-transfer results and is similar to figure 21 showing skin-friction results. The surface shown was obtained from the Sommer and Short theory along with the Colburn analogy. The incompressible Stanton number was found from the Karmen-Schoenherr theory of incompressible local skin friction along with the Colburn analogy. There seem to be no distinct trends evident from the experimental data (refs. 2, 21, 22, and 24 to 27). Contrary to the skin-friction results (fig. 21) there is no discernible Reynolds number trend. Reduced heat flowmeter data are presented in table 4.

CONCLUSIONS

An investigation of the turbulent boundary layer on a hollow cylinder at a Mach number of 6, at Reynolds numbers up to 29×10^6, and at two wall-temperature ratios leads to the following conclusions:

1. At high Reynolds number, the theory of Spalding and Chi gives fair agreement with the experimental data.

2. The wall-temperature ratio does not seem to have an appreciable effect on the average skin-friction coefficient at high Reynolds numbers.

3. Use of the Colburn modification of Reynolds analogy along with the turbulent skin-friction theory of Spalding and Chi, which was found to agree best with the

experimental skin-friction data at high Reynolds numbers, underestimates the experimentally measured heat-transfer coefficients.

Langley Research Center,
National Aeronautics and Space Administration,
Langley Station, Hampton, Va., October 15, 1966,
129-01-09-04-23.

REFERENCES

1. Adcock, Jerry B.; Peterson, John B., Jr.; and McRee, Donald I.: Experimental Investigation of a Turbulent Boundary Layer at Mach 6, High Reynolds Numbers, and Zero Heat Transfer. NASA TN D-2907, 1965.

2. Winkler, Eva M.; and Cha, Moon H.: Investigation of Flat Plate Hypersonic Turbulent Boundary Layers With Heat Transfer at a Mach Number of 5.2. NAVORD Rept. 6631, U.S. Naval Ord. Lab., Sept. 15, 1959.

3. Danberg, James E.: Characteristics of the Turbulent Boundary Layer With Heat and Mass Transfer at M=6.7. NOLTR 64-99, U.S. Navy, Oct. 19, 1964.

4. Sommer, Simon C.; and Short, Barbara J.: Free-Flight Measurements of Turbulent-Boundary-Layer Skin Friction in the Presence of Severe Aerodynamic Heating at Mach Numbers From 2.8 to 7.0. NACA TN 3391, 1955.

5. Monaghan, R. J.; and Johnson, J. E.: The Measurement of Heat Transfer and Skin Friction at Supersonic Speeds. Part II – Boundary Layer Measurements on a Flat Plate at M=2.5 and Zero Heat Transfer. C.P. No. 64, Brit. A.R.C., 1952.

6. Van Driest, E. R.: The Turbulent Boundary Layer With Variable Prandtl Number. Rept. No. AL-1914, North Am. Aviation, Inc., Apr. 2, 1954.

7. Spalding, D. B.; and Chi, S. W.: The Drag of a Compressible Turbulent Boundary Layer on a Smooth Flat Plate With and Without Heat Transfer. J. Fluid Mech., vol. 18, pt. 1, Jan. 1964, pp. 117-143.

8. Colburn, Allan P.: A Method of Correlating Forced Convection Heat Transfer Data and a Comparison With Fluid Friction. Trans. Am. Inst. Chem. Engrs., vol. XXIX, 1933, pp. 174-211.

9. Sterrett, James R.; and Emery, James C.: Extension of Boundary-Layer-Separation Criteria to a Mach Number of 6.5 by Utilizing Flat Plates With Forward-Facing Steps. NASA TN D-618, 1960.

10. Beckwith, Ivan E.; and Gallagher, James J.: Heat Transfer and Recovery Temperatures on a Sphere With Laminar, Transitional, and Turbulent Boundary Layers at Mach Numbers of 2.00 and 4.15. NACA TN 4125, 1957.

11. Donaldson, Coleman duP.: Heat Transfer and Skin Friction for Turbulent Boundary Layers on Heated or Cooled Surfaces at High Speeds. NACA RM L52H04, 1952.

12. Van Driest, E. R.: Investigation of Laminar Boundary Layer in Compressible Fluids Using the Crocco Method. NACA TN 2597, 1952.

13. Lobb, R. Kenneth; Winkler, Eva M.; and Persh, Jerome: Experimental Investigation of Turbulent Boundary Layers in Hypersonic Flow. J. Aeron. Sci., vol. 22, no. 1, Jan. 1955, pp. 1-9, 50. (NAVORD Rept. 3880.)

14. Wilson, R. E.: Characteristics of Turbulent Boundary Layer Flow Over a Smooth, Thermally Insulated Flat Plate at Supersonic Speeds. DRL-301, CM-712 (Contract NOrd-9195), Univ. of Texas, June 1, 1952.

15. Peterson, John B., Jr.: A Comparison of Experimental and Theoretical Results for the Compressible Turbulent-Boundary-Layer Skin Friction With Zero Pressure Gradient. NASA TN D-1795, 1963.

16. Chapman, Dean R.; and Kester, Robert H.: Turbulent Boundary-Layer and Skin-Friction Measurements in Axial Flow Along Cylinders at Mach Numbers Between 0.5 and 3.6. NACA TN 3097, 1954.

17. Swanson, Andrew G.; Buglia, James J.; and Chauvin, Leo T.: Flight Measurements of Boundary-Layer Temperature Profiles on a Body of Revolution (NACA RM-10) at Mach Numbers From 1.2 to 3.5. NACA TN 4061, 1957.

18. Korkegi, Robert H.: Transition Studies and Skin-Friction Measurements on an Insulated Flat Plate at a Mach Number of 5.8. J. Aeron. Sci., vol. 23, no. 2, Feb. 1956, pp. 97-107, 192.

19. Brinich, Paul F.; and Diaconis, Nick S.: Boundary-Layer Development and Skin Friction at Mach Number 3.05. NACA TN 2742, 1952.

20. Hill, F. K.: Appendix II – Skin Friction and Heat Transfer Measurements at Mach Numbers From 8-10 in Turbulent Boundary Layers. Bumblebee Aerodynamics Panel. TG-14-37, vol. I, Appl. Phys. Lab., Johns Hopkins Univ., May 1959, pp. 15-26.

21. Neal, Luther, Jr.: A Study of the Pressure, Heat Transfer, and Skin Friction on Sharp and Blunt Flat Plates at Mach 6.8. NASA TN D-3312, 1966.

22. Maloney, Joseph P.: Drag and Heat Transfer on a Parabolic Body of Revolution (NACA RM-10) in Free Flight to Mach Number 2 With Both Constant and Varying Reynolds Number and Heating Effects on Turbulent Skin Friction. NACA RM L54D06, 1954.

23. Pappas, C. C.: Measurement of Heat Transfer in the Turbulent Boundary Layer on a Flat Plate in Supersonic Flow and Comparison With Skin-Friction Results. NACA TN 3222, 1954.

24. Tendeland, Thorval: Effects of Mach Number and Wall-Temperature Ratio on Turbulent Heat Transfer at Mach Numbers From 3 to 5. NASA TR R-16, 1959. (Supersedes NACA TN 4236.)

25. Rumsey, Charles B.; and Lee, Dorothy B.: Measurements of Aerodynamic Heat Transfer on a 15° Cone-Cylinder-Flare Configuration in Free Flight at Mach Numbers Up to 4.7. NASA TN D-824, 1961.

26. Holloway, Paul F.; and Sterrett, James R.: Effect of Controlled Surface Roughness on Boundary-Layer Transition and Heat Transfer at Mach Numbers of 4.8 and 6.0. NASA TN D-2054, 1964.

27. Slack, Ellis G.: Experimental Investigation of Heat Transfer Through Laminar and Turbulent Boundary Layers on a Cooled Flat Plate at a Mach Number of 2.4. NACA TN 2686, 1952.

TABLE 1.- BOUNDARY-LAYER PRESSURE, MACH NUMBER, AND VELOCITY DISTRIBUTIONS

(a) Station 1: x_{le} = 8.0 in. (20.3 cm); T_δ = 110° R (61° K); T_t = 874° R (486° K); M_δ = 5.92; p_δ = 0.359 psia (2.47 kN/m^2); p_t = 522 psia (3.60 MN/m^2); and T_w/T_{aw} = 0.50

y, in.	y, cm	$\frac{p_\delta}{p'}$	$\frac{M}{M_\delta}$	$\frac{u}{u_\delta}$
0.0039	0.0099	0.2876	0.261	0.480
.0041	.0104	.2623	.271	.495
.0107	.0272	.1405	.384	.691
.0126	.0320	.1067	.444	.751
.0188	.0478	.0784	.522	.824
.0275	.0699	.0718	.546	.851
.0355	.0902	.0653	.574	.873
.0421	.1069	.0600	.599	.890
.0524	.1331	.0514	.649	.916
.0669	.1699	.0439	.703	.943
.0780	.1981	.0390	.748	.959
.1030	.2616	.0311	.838	.985
.1304	.3312	.0256	.927	1.003
.1580	.4013	.0232	.974	1.002
.1980	.5029	.0223	.993	.999
.2390	.6071	.0220	.999	1.000
.2829	.7186	.0219	1.000	1.000

TABLE 1.- BOUNDARY-LAYER PRESSURE, MACH NUMBER, AND VELOCITY DISTRIBUTIONS – Continued

(b) Station 2: x_{le} = 11.0 in. (27.9 cm); T_δ = 109° R (60° K); T_t = 875° R (486° K); M_δ = 5.94; p_δ = 0.352 psia (2.43 kN/m^2); p_t = 523 psia (3.61 MN/m^2); and T_w/T_{aw} = 0.50

y, in.	y, cm	$\frac{p_\delta}{p'}$	$\frac{M}{M_\delta}$	$\frac{u}{u_\delta}$
0.0035	0.0089	0.2729	0.265	0.502
.0035	.0089	.2764	.262	.497
.0035	.0089	.2744	.263	.499
.0046	.0117	.2330	.289	.552
.0069	.0175	.1796	.333	.630
.0112	.0284	.1392	.384	.695
.0153	.0389	.1097	.436	.742
.0215	.0546	.0918	.479	.780
.0322	.0818	.0863	.495	.802
.0406	.1031	.0783	.521	.826
.0512	.1300	.0665	.565	.858
.0634	.1610	.0592	.601	.884
.0996	.2530	.0509	.650	.911
.1271	.3228	.0422	.715	.943
.1545	.3924	.0338	.801	.976
.1926	.4892	.0282	.878	.995
.2305	.5855	.0242	.948	1.003
.2668	.6777	.0225	.984	1.000
.3194	.8113	.0219	1.002	1.001

TABLE 1.- BOUNDARY-LAYER PRESSURE, MACH NUMBER, AND VELOCITY DISTRIBUTIONS – Continued

(c) Station 3: x_{le} = 33.0 in. (83.8 cm); T_δ = 108° R (60° K); T_t = 878° R (488° K); M_δ = 5.98; p_δ = 0.340 psia (2.34 kN/m^2); p_t = 523 psia (3.61 MN/m^2); and T_w/T_{aw} = 0.50

y, in.	y, cm	$\frac{p_\delta}{p'}$	$\frac{M}{M_\delta}$	$\frac{u}{u_\delta}$
0.0035	0.0089	0.3253	0.235	0.420
.0035	.0089	.3012	.247	.434
.0035	.0089	.3169	.239	.425
.0035	.0089	.2962	.249	.437
.0044	.0112	.2673	.265	.476
.0070	.0178	.1918	.320	.555
.0154	.0391	.1320	.393	.688
.0284	.0721	.1167	.420	.728
.0411	.1044	.1091	.435	.748
.0534	.1356	.1013	.452	.767
.0664	.1687	.0925	.474	.789
.0930	.2362	.0795	.513	.824
.1214	.3084	.0695	.550	.855
.1609	.4087	.0587	.600	.889
.2101	.5337	.0481	.665	.921
.2751	.6988	.0372	.758	.964
.3381	.8588	.0299	.847	.989
.4038	1.0257	.0246	.935	1.003
.4673	1.1869	.0222	.985	1.006
.5286	1.3426	.0216	.999	1.001
.5932	1.5067	.0215	1.001	1.000

TABLE 1.- BOUNDARY-LAYER PRESSURE, MACH NUMBER, AND VELOCITY DISTRIBUTIONS – Continued

(d) Station 4: x_{le} = 37 in. (94.0 cm); T_δ = 107° R (59° K); T_t = 869° R (483° K); M_δ = 5.98; p_δ = 0.339 psia (2.34 kN/m^2); p_t = 523 psia (3.61 MN/m^2); and T_w/T_{aw} = 0.50

y, in.	y, cm	$\frac{p_\delta}{p'}$	$\frac{M}{M_\delta}$	$\frac{u}{u_\delta}$
0.0035	0.0089	0.3231	0.236	0.420
.0036	.0091	.2976	.249	.438
.0049	.0124	.2863	.254	.456
.0052	.0132	.3036	.246	.452
.0065	.0165	.2792	.258	.487
.0077	.0196	.2522	.274	.506
.0096	.0244	.2233	.294	.554
.0121	.0307	.1779	.334	.625
.0138	.0351	.1517	.364	.659
.0204	.0518	.1257	.403	.707
.0306	.0777	.1148	.423	.733
.0375	.0953	.1117	.429	.742
.0476	.1209	.1037	.446	.760
.0628	.1595	.0941	.470	.785
.0753	.1913	.0869	.490	.804
.1007	.2558	.0756	.526	.835
.1277	.3244	.0674	.559	.865
.1766	.4486	.0548	.622	.902
.2312	.5872	.0445	.692	.939
.2905	.7379	.0355	.776	.971
.3594	.9129	.0287	.864	.992
.4211	1.0696	.0239	.948	1.004
.4888	1.2416	.0217	.997	1.003
.5503	1.3978	.0213	1.004	1.001
.6139	1.5593	.0216	.998	.999

TABLE 1.- BOUNDARY-LAYER PRESSURE, MACH NUMBER, AND VELOCITY DISTRIBUTIONS – Continued

(e) Station 5: x_{le} = 40.0 in. (101.6 cm); T_δ = 107° R (59° K); T_t = 872° R (484° K); M_δ = 5.97; p_δ = 0.342 psia (2.36 kN/m^2); p_t = 523 psia (3.61 MN/m^2); and T_w/T_{aw} = 0.50

y, in.	y, cm	$\frac{p_\delta}{p'}$	$\frac{M}{M_\delta}$	$\frac{u}{u_\delta}$
0.0035	0.0089	0.3356	0.231	0.410
.0051	.0130	.2872	.254	.457
.0094	.0239	.2253	.293	.547
.0175	.0445	.1370	.385	.685
.0193	.0490	.1256	.404	.705
.0305	.0775	.1130	.427	.734
.0389	.0988	.1091	.435	.745
.0516	.1311	.1013	.453	.765
.0600	.1524	.0955	.467	.779
.0725	.1842	.0892	.484	.796
.0850	.2159	.0832	.502	.812
.0996	.2530	.0779	.519	.827
.1149	.2918	.0729	.537	.843
.1633	.4148	.0595	.597	.886
.2246	.5705	.0476	.669	.927
.2894	.7351	.0379	.752	.962
.3531	.8969	.0309	.834	.986
.4184	1.0627	.0255	.918	1.002
.4799	1.2189	.0227	.975	1.005
.5452	1.3848	.0217	.995	1.002
.6076	1.5433	.0215	1.002	1.001

TABLE 1.- BOUNDARY-LAYER PRESSURE, MACH NUMBER, AND VELOCITY DISTRIBUTIONS – Continued

(f) Station 1: x_{le} = 8.0 in. (20.3 cm); T_δ = 119° R (66° K); T_t = 974° R (541° K); M_δ = 5.99; p_δ = 0.334 psia (2.30 kN/m^2); p_t = 523 psia (3.61 MN/m^2); and T_w/T_{aw} = 0.44

y, in.	y, cm	$\frac{p_\delta}{p'}$	$\frac{M}{M_\delta}$	$\frac{u}{u_\delta}$
0.0035	0.0089	0.3080	0.243	0.461
.0035	.0089	.2877	.254	.474
.0040	.0102	.2457	.278	.512
.0057	.0145	.1587	.356	.609
.0099	.0251	.1029	.448	.714
.0207	.0526	.0715	.542	.820
.0266	.0676	.0617	.585	.855
.0318	.0808	.0607	.590	.866
.0475	.1207	.0508	.646	.904
.0603	.1532	.0432	.702	.933
.0759	.1928	.0370	.760	.960
.1050	.2667	.0292	.856	.989
.1349	.3427	.0241	.944	1.007
.1600	.4064	.0222	.985	1.008
.1979	.5027	.0216	.999	1.000
.2384	.6055	.0215	1.002	1.001

TABLE 1.- BOUNDARY-LAYER PRESSURE, MACH NUMBER, AND VELOCITY DISTRIBUTIONS – Continued

(g) Station 2: x_{le} = 11.0 in. (27.9 cm); T_δ = 120° R (67° K); T_t = 979° R (544° K); M_δ = 5.98; p_δ = 0.338 psia (2.33 kN/m^2); p_t = 522 psia (3.60 MN/m^2); and T_w/T_{aw} = 0.44

$\frac{y}{in.}$	$\frac{y}{cm}$	$\frac{p_\delta}{p'}$	$\frac{M}{M_\delta}$	$\frac{u}{u_\delta}$
0.0035	0.0089	0.3133	0.240	0.418
.0035	.0089	.3026	.246	.426
.0047	.0119	.2226	.294	.494
.0060	.0152	.1751	.336	.558
.0111	.0282	.1185	.414	.698
.0176	.0447	.0913	.476	.769
.0259	.0658	.0781	.517	.807
.0362	.0919	.0723	.538	.830
.0512	.1300	.0632	.577	.859
.0639	.1623	.0557	.615	.887
.0893	.2268	.0433	.700	.935
.1145	.2908	.0353	.777	.967
.1399	.3553	.0298	.846	.988
.1906	.4841	.0237	.951	1.004
.2413	.6129	.0214	1.001	1.002
.2917	.7409	.0215	.999	1.000
.3574	.9078	.0215	.999	1.000

TABLE 1.- BOUNDARY-LAYER PRESSURE, MACH NUMBER, AND VELOCITY DISTRIBUTIONS – Continued

(h) Station 3: x_{le} = 33.0 in. (83.8 cm); T_δ = 114° R (63° K); T_t = 957° R (532° K); M_δ = 6.08; p_δ = 0.304 psia (2.10 kN/m^2); p_t = 522 psia (3.60 MN/m^2); and T_w/T_{aw} = 0.44

y, in.	y, cm	$\frac{p_\delta}{p'}$	$\frac{M}{M_\delta}$	$\frac{u}{u_\delta}$
0.0035	0.0089	0.2595	0.265	0.446
.0035	.0089	.2592	.265	.446
.0036	.0091	.2349	.281	.463
.0036	.0091	.2180	.293	.475
.0078	.0198	.1680	.339	.585
.0093	.0236	.1462	.365	.631
.0201	.0511	.1109	.423	.720
.0285	.0724	.1011	.444	.744
.0416	.1057	.0979	.452	.758
.0542	.1377	.0928	.465	.773
.0687	.1745	.0856	.485	.791
.0917	.2329	.0772	.512	.816
.1152	.2926	.0680	.547	.843
.1531	.3889	.0572	.598	.882
.2045	.5194	.0468	.663	.921
.2526	.6416	.0385	.732	.951
.3072	.7803	.0317	.808	.978
.3556	.9032	.0271	.874	.993
.4166	1.0582	.0231	.948	1.001
.4797	1.2184	.0214	.986	1.001
.5350	1.3589	.0209	.997	1.000
.6062	1.5397	.0207	1.001	1.001

TABLE 1.- BOUNDARY-LAYER PRESSURE, MACH NUMBER, AND VELOCITY DISTRIBUTIONS – Concluded

(i) Station 4: x_{le} = 37.0 in. (94.0 cm); T_δ = 118° R (66° K); T_t = 978° R (543° K); M_δ = 6.04; p_δ = 0.320 psia (2.21 kN/m^2); p_t = 524 psia (3.61 MN/m^2); and T_w/T_{aw} = 0.44

y, in.	y, cm	$\frac{p_\delta}{p'}$	$\frac{M}{M_\delta}$	$\frac{u}{u_\delta}$
0.0035	0.0089	0.3516	0.222	0.382
.0035	.0089	.3455	.224	.385
.0064	.0163	.2645	.264	.476
.0106	.0269	.1773	.332	.605
.0121	.0307	.1523	.360	.642
.0190	.0483	.1302	.392	.690
.0275	.0699	.1140	.420	.723
.0401	.1019	.1085	.432	.740
.0528	.1341	.1021	.446	.756
.0632	.1605	.0952	.462	.771
.0927	.2355	.0826	.498	.807
.1181	.3000	.0728	.532	.833
.1457	.3701	.0646	.565	.860
.2005	.5093	.0518	.634	.905
.2513	.6383	.0428	.699	.938
.3019	.7668	.0359	.764	.964
.3627	.9213	.0294	.846	.988
.4304	1.0932	.0243	.932	1.001
.4916	1.2487	.0218	.985	1.003
.5549	1.4094	.0211	1.001	1.001
.6347	1.6121	.0218	.998	1.000

TABLE 2

DATA REDUCTION FOR PRESSURE-SURVEY MEASUREMENTS

T_w/T_{aw}	Run	x_{le}, in.	x_{le}, cm	x, in.	x, cm	M_δ	p_t, psia	p_t, MN/m^2	T_t, ^oR	T_t, ^oK	δ_p, in.	δ_p, cm	θ, in.	θ, cm	R_θ	R_x	C_F
0.44	492	8.0	20.3	4.3	10.9	5.99	522.7	3.607	974.1	541.0	0.153	0.389	4.32×10^{-3}	10.97×10^{-3}	3.10×10^3	2.97×10^6	2.09×10^{-3}
	491	11.0	27.9	7.3	18.5	5.98	522.2	3.604	979.3	544.1	.205	.521	6.29	15.98	4.29	4.95	1.73
	530	33.0	83.8	29.3	74.4	6.08	522.2	3.606	956.8	531.6	.465	1.181	15.10	38.35	10.61	19.61	1.08
	580	37.0	94.0	33.3	84.6	6.04	524.4	3.616	977.5	543.1	.488	1.240	16.90	42.93	11.62	22.15	1.05
	570	40.0	101.6	36.3	92.2	6.06	524.1	3.614	970.0	538.9	.509	1.293	17.40	44.20	11.81	24.10	.98
0.50	622	8.0	20.3	2.9	8.4	5.92	521.8	3.597	874.4	486.0	0.156	0.396	4.07×10^{-3}	10.34×10^{-3}	3.60×10^3	2.40×10^6	3.00×10^{-3}
	621	11.0	27.9	5.9	15.0	5.94	522.6	3.603	875.0	486.1	.210	.533	6.15	15.62	5.18	4.86	2.13
	593	33.0	83.8	27.9	70.9	5.98	523.3	3.608	877.5	487.5	.460	1.168	14.70	37.34	12.91	22.91	1.13
	592	37.0	94.0	31.9	81.0	5.98	523.0	3.606	868.9	482.7	.470	1.194	15.90	40.39	12.87	26.90	.96
	591	40.0	101.6	34.9	88.6	5.97	523.4	3.609	871.6	484.2	.495	1.257	15.90	40.39	13.42	28.66	.94

TABLE 3.- TEMPERATURE SURVEY

(a) Station 3: x_{le} = 33 in. (83.8 cm); M_δ = 5.98; p_t = 523 psia (3.61 MN/m^2); and T_w/T_{aw} = 0.50

y, in.	y, cm	$T_{t,\delta}$, ^oR	$T_{t,\delta}$, ^oK	T_p, ^oR	T_p, ^oK	T_t, ^oR	T_t, ^oK
0.0100	0.0254	871	484	581	323	618	343
.0110	.0279	868	482	623	346	663	368
.0124	.0315	868	482	643	357	685	381
.0195	.0495	867	482	669	372	715	397
.0250	.0635	865	481	681	378	728	404
.0324	.0823	865	481	687	382	734	408
.0450	.1143	866	481	699	388	747	415
.0590	.1499	863	479	713	396	763	424
.0873	.2217	865	481	735	408	788	438
.1110	.2819	864	480	750	417	804	447
.1371	.3482	863	479	765	425	820	456
.1606	.4709	863	479	778	432	833	463
.2137	.5428	863	479	803	446	859	477
.2621	.6657	864	480	823	457	875	486
.3151	.8004	863	479	838	466	885	492
.3760	.9550	864	480	847	471	888	493
.4416	1.1217	862	479	840	467	879	488
.5006	1.2715	863	479	833	463	868	482
.5681	1.4430	862	479	830	461	863	479
.6932	1.7607	871	484	838	466	871	484

TABLE 3.- TEMPERATURE SURVEY – Continued

(b) Station 4: x_{le} = 37 in. (94.0 cm); M_δ = 5.98; p_t = 523 psia (3.61 MN/m^2); and T_w/T_{aw} = 0.50

y, in.	y, cm	$T_{t,\delta}$, ^oR	$T_{t,\delta}$, ^oK	T_p, ^oR	T_p, ^oK	T_t, ^oR	T_t, ^oK
0.0102	0.0259	892	496	573	318	606	337
.0116	.0295	896	498	595	331	630	350
.0145	.0368	870	483	650	361	691	384
.0185	.0470	869	483	664	369	709	394
.0270	.0686	869	483	676	376	723	402
.0312	.0792	871	484	683	379	730	406
.0397	.1006	874	486	692	384	741	412
.0481	.1222	873	485	700	389	749	416
.0607	.1542	873	485	713	396	763	424
.0722	.1834	874	486	723	402	774	430
.0977	.2482	877	487	743	413	796	442
.1239	.3147	877	487	759	422	814	452
.1747	.4437	876	487	786	437	842	468
.2254	.5725	878	488	811	451	866	481
.2773	.7043	878	488	832	462	883	491
.3369	.8557	879	488	850	472	896	498
.4065	1.0325	879	488	860	478	898	499
.4656	1.1826	879	488	855	475	893	496
.5306	1.3477	875	486	844	469	880	489
.5942	1.5093	872	484	839	466	874	486
.6549	1.6634	872	484	837	465	872	484
.6933	1.7609	872	484	838	466	872	484

TABLE 3.- TEMPERATURE SURVEY – Continued

(c) Station 5: x_{le} = 40 in. (101.6 cm); M_δ = 5.97; p_t = 523 psia (3.61 MN/m^2); and T_w/T_{aw} = 0.50

y, in.	y, cm	$T_{t,\delta}$, °R	$T_{t,\delta}$, °K	T_p, °R	T_p, °K	T_t, °R	T_t, °K
0.0101	0.0257	873	485	578	321	611	339
.0101	.0257	873	485	590	328	624	347
.0142	.0361	874	486	647	359	688	382
.0158	.0401	873	485	657	365	700	389
.0228	.0579	873	485	676	376	722	401
.0270	.0686	871	484	681	378	728	404
.0354	.0899	873	485	690	383	738	410
.0521	.1323	895	497	707	393	757	421
.0579	.1471	873	485	713	396	763	424
.0706	.1793	873	485	723	402	774	430
.0836	.2123	874	486	734	408	786	437
.1112	.2824	874	486	750	417	804	447
.1365	.3467	872	484	764	424	819	455
.1745	.4432	873	485	784	436	840	467
.2377	.6038	875	486	812	451	865	481
.3011	.7648	873	485	833	463	882	490
.3642	.9251	873	485	848	471	891	495
.4276	1.0861	873	485	856	456	894	497
.4890	1.2420	874	486	851	473	889	494
.5563	1.4130	873	485	843	468	880	489
.6187	1.5715	874	486	840	467	874	486

TABLE 3.- TEMPERATURE SURVEY – Continued

(d) Station 1: x_{le} = 8.0 in. (20.3 cm); M_δ = 5.99; p_t = 523 psia (3.61 MN/m^2); and T_w/T_{aw} = 0.44

y, in.	y, cm	$T_{t,\delta}$, ^oR	$T_{t,\delta}$, ^oK	T_p, ^oR	T_p, ^oK	T_t, ^oR	T_t, ^oK
0.0100	0.0254	962	534	675	375	721	401
.0123	.0312	967	537	709	394	758	421
.0164	.0417	970	539	730	406	782	434
.0183	.0464	972	540	766	426	822	457
.0271	.0688	975	542	825	458	885	492
.0325	.0826	974	541	835	464	896	498
.0395	.1003	976	542	852	473	915	508
.0438	.1113	976	542	864	480	927	515
.0606	.1539	976	542	894	497	957	532
.0733	.1862	977	543	915	508	976	542
.0884	.2245	977	543	932	518	989	549
.1153	.2929	977	543	954	530	1004	558
.1303	.3310	977	543	961	534	1006	559
.1598	.4059	977	543	960	533	1001	556
.1954	.4963	977	543	949	527	989	549
.2277	.5784	978	543	944	524	983	546
.2570	.6528	977	543	942	523	981	545
.3389	.8608	979	544	943	524	979	544

TABLE 3.- TEMPERATURE SURVEY – Continued

(e) Station 2: x_{le} = 11.0 in. (27.9 cm); M_δ = 5.98; p_t = 523 psia (3.61 MN/m^2); and T_w/T_{aw} = 0.44

y, in.	y, cm	$T_{t,\delta}$, °R	$T_{t,\delta}$, °K	T_p, °R	T_t, °K	T_t, °R	T_t, °K
0.0100	0.0254	959	533	683	379	730	406
.0103	.0262	969	538	687	382	735	408
.0142	.0361	974	541	737	409	790	439
.0180	.0457	977	543	766	426	821	456
.0207	.0526	981	545	780	433	837	465
.0291	.0739	983	546	803	446	862	479
.0350	.0889	988	549	818	454	878	488
.0436	.1107	989	549	834	463	895	497
.0629	.1598	991	551	869	483	932	518
.0802	.2037	993	552	897	498	960	533
.1031	.2619	995	553	932	518	993	552
.1291	.3279	968	538	933	518	987	548
.1578	.4008	985	547	964	536	1013	563
.2213	.5621	986	548	960	533	1001	556
.2741	.6962	990	550	955	531	995	553
.3246	.8245	992	551	956	531	992	551
.3836	.9743	994	552	958	532	994	552

TABLE 3.- TEMPERATURE SURVEY – Continued

(f) Station 3: x_{le} = 33.0 in. (83.8 cm); M_δ = 6.08; p_t = 524 psia (3.61 MN/m^2); and T_w/T_{aw} = 0.44

y, in.	y, cm	$T_{t,\delta}$, °R	$T_{t,\delta}$, °K	T_p, °R	T_p, °K	T_t, °R	T_t, °K
0.0100	0.0254	960	533	635	353	678	433
.0128	.0325	959	533	684	380	732	407
.0169	.0429	982	546	702	390	753	418
.0255	.0648	960	533	732	407	786	437
.0338	.0859	982	546	753	418	809	449
.0381	.0968	986	548	763	424	819	455
.0509	.1293	990	550	781	434	839	466
.0793	.2014	992	551	814	452	875	486
.0902	.2291	989	549	819	455	881	489
.1479	.3757	979	544	857	476	921	512
.1746	.4435	989	549	880	489	945	525
.2255	.5728	966	537	891	495	953	529
.2751	.6988	964	536	913	507	972	540
.3363	.8542	961	534	932	518	984	547
.4030	1.0236	960	533	937	521	981	545
.4684	1.1897	954	530	923	513	963	535
.5316	1.3503	954	530	915	508	954	530
.5907	1.5004	953	529	914	508	952	529
.6582	1.6718	953	529	914	508	953	529
.7362	1.8699	952	529	913	507	952	529

TABLE 3.- TEMPERATURE SURVEY – Continued

(g) Station 4: x_{le} = 37.0 in. (94.0 cm); M_δ = 6.04; p_t = 524 psia (3.61 MN/m^2); and T_w/T_{aw} = 0.44

y, in.	y, cm	$T_{t,\delta}$, ^oR	$T_{t,\delta}$, ^oK	T_p, ^oR	T_p, ^oK	T_t, ^oR	T_t, ^oK
0.0100	0.0254	886	492	601	334	640	356
.0200	.0508	987	548	736	409	788	438
.0300	.0762	997	554	757	421	812	451
.0400	.1016	987	548	771	428	827	459
.0500	.1270	988	549	782	434	839	466
.1000	.2540	1002	557	830	461	892	496
.1500	.3810	996	553	861	478	925	514
.2000	.5080	989	549	890	494	955	531
.2500	.6350	994	552	916	509	982	546
.3000	.7620	992	551	935	519	1000	556
.3500	.8890	992	551	956	531	1013	563
.4000	1.0160	987	548	957	532	1007	559
.4500	1.1430	980	544	951	528	997	554
.5000	1.2700	987	548	954	530	996	553
.5500	1.3970	982	546	945	525	985	547
.6000	1.5240	994	552	954	530	994	552

TABLE 3.- TEMPERATURE SURVEY – Concluded

(h) Station 5: x_{le} = 40.0 in. (101.6 cm); M_δ = 6.06; p_t = 523 psia (3.61 MN/m^2); and T_w/T_{aw} = 0.44

y, in.	y, cm	$T_{t,\delta}$, °R	$T_{t,\delta}$, °K	T_p, °R	T_p, °K	T_t, °R	T_t, °K
0.0100	0.0254	984	547	600	333	642	357
.0105	.0267	990	550	649	361	694	386
.0131	.0333	968	538	705	392	755	419
.0165	.0419	993	552	710	394	760	422
.0192	.0488	996	553	741	412	794	441
.0280	.0711	997	554	758	421	813	452
.0358	.0909	985	547	766	426	823	457
.0425	.1080	991	551	770	428	827	459
.0509	.1293	994	552	780	433	838	466
.0620	.1575	995	553	794	441	853	474
.0890	.2261	995	553	819	455	880	489
.1185	.3010	999	555	833	463	895	497
.1414	.3592	995	553	851	473	915	508
.1903	.4834	997	554	884	491	949	527
.2390	.6071	1001	556	912	507	976	542
.2903	.7374	1002	557	937	521	998	554
.3441	.8740	992	551	957	532	1014	563
.4053	1.0295	974	541	964	536	1014	563
.4687	1.1905	974	541	951	528	995	553
.5321	1.3515	983	546	950	528	990	550
.6010	1.5265	979	544	942	523	980	544

TABLE 4

REDUCED HEAT FLOWMETER DATA

$\frac{T_w}{T_{aw}}$	Station	Run	x_{le}', in.	x_{le}', cm	x, in.	x, cm	M_δ	p_t, psia	p_t, MN/m^2	T_t, ^oR	T_t, ^oK	q/S, Btu/ft^2-sec	q/S, kW/m^2	N_{St}
0.44	1	411	12.0	30.5	8.3	21.08	5.98	522.8	3.605	989.0	549.4	2.55	28.943	0.865×10^{-3}
	2		24.0	61.0	20.3	51.56	6.01					2.52	28.502	.881
	3		36.0	91.4	32.3	82.04	6.02					2.19	24.857	.762
	1	412	12.0	30.48	8.3	21.08	5.98	522.0	3.599	989.2	549.5	2.46	27.921	.831
	2		24.0	60.96	20.3	51.56	6.01					2.37	26.900	.831
	3		36.0	91.44	32.3	82.04	6.02					2.10	23.835	.750
	1	420	12.0	30.48	8.3	21.08	5.98	523.2	3.607	983.1	546.2	2.53	28.716	.856
	2		24.0	60.96	20.3	51.56	6.01					2.50	28.375	.871
	3		36.0	91.44	32.3	82.04	6.02					2.09	23.722	.727
	1	430	12.0	30.48	8.3	21.08	5.98	523.9	3.612	960.8	533.8	2.60	29.510	.898
	2		24.0	60.96	20.3	51.56	6.01					2.47	28.035	.879
	3		36.0	91.44	32.3	82.04	6.02					2.17	24.630	.769
	1	470	12.0	30.48	8.3	21.08	5.98	522.4	3.602	974.7	541.5	2.57	29.170	.868
	2		24.0	60.96	20.3	51.56	6.01					2.82	32.007	.991
	3		36.0	91.44	32.3	82.04	6.02					2.28	25.878	.845
	1	491	12.0	30.48	8.3	21.08	5.98	522.7	3.604	974.1	541.2	2.48	28.148	.842
	2		24.0	60.96	20.3	51.56	6.01					2.50	28.375	.874
	3		36.0	91.44	32.3	82.04	6.02					2.17	24.630	.767
	1	492	12.0	30.48	8.3	21.08	5.98	522.2	3.601	979.4	544.1	2.62	29.737	.888
	2		24.0	60.96	20.3	51.56	6.01					2.68	30.418	.943
	3		36.0	91.44	32.3	82.04	6.02					2.22	25.197	.801
	1	500	12.0	30.48	8.3	21.08	5.98	523.3	3.608	977.6	543.1	2.35	26.673	.812
	2		24.0	60.96	20.3	51.56	6.01					2.58	29.283	.924
	3				32.3	82.04	6.02	----	----	----	----	---	-----	---
	1	510	12.0	30.48	8.3	21.08	5.98	524.5	3.616	990.5	550.3	2.42	27.467	.817
	2		24.0	60.96	20.3	51.56	6.01					2.42	27.467	.845
	3		---	----	---	----	---	----	----	----	----	---	-----	---
	1	520	12.0	30.48	8.3	21.08	5.98	524.4	3.616	978.9	543.8	2.55	28.993	.856
	2		24.0	60.96	20.3	51.56						2.61	29.624	.906
	3		---	----	---	----	---	----	----	----	----	---	-----	---
	1	530	12.0	30.48	8.3	21.08	5.98	521.9	3.599	956.8	531.6	2.16	24.516	.745
	2		24.0	60.96	20.3	51.56	6.01					2.42	27.467	.861
	3	---	---	---	----	---	----	---	----	----	----	---	-----	---
	1	570	12.0	30.48	8.3	21.08	5.98	524.3	3.615	959.6	533.1	2.37	26.900	.813
	2		24.0	60.96	20.3	51.56	6.01					2.58	29.283	.924
	3		36.0	91.44	32.3	82.04	6.02					1.73	19.636	.632
0.50	1	401	12.0	30.5	6.9	17.5	5.98	523.1	3.607	876.1	486.7	2.09	23.72	0.838×10^{-3}
	2		24.0	61.0	18.9	48.0	6.01					2.02	22.93	.829
	3		36.0	91.4	30.9	78.5	6.02					1.57	17.82	.648
	1	402	12.0	30.5	6.9	17.5	5.98	522.3	3.601	872.7	484.8	2.01	22.81	.806
	2		24.0	61.0	18.9	48.0	6.01					1.99	22.59	.825
	3		36.0	91.4	30.9	78.5	6.02					1.62	18.39	.681
	1	403	12.0	30.5	6.9	17.5	5.98	522.7	3.604	865.0	480.6	1.93	21.91	.814
	2		24.0	61.0	18.9	48.0	6.01					1.85	21.00	.805
	3		36.0	91.4	30.9	78.5	6.02					1.59	18.05	.701
	1	591	12.0	30.5	6.9	17.5	5.98	523.4	3.609	871.6	484.2	2.03	23.04	.825
	2		24.0	61.0	18.9	48.0	6.01					1.99	22.59	.840
	3		---	---	---	---	---	----	----	----	----	---	----	---
	1	592	12.0	30.5	6.9	17.5	5.98	523.0	3.606	868.9	482.7	2.01	22.81	.826
	2		24.0	61.0	18.9	48.0	6.01					1.99	22.59	.848
	3		---	---	---	---	---	----	----	----	----	---	----	---
	1	593	12.0	30.5	6.9	17.5	5.98	523.3	3.608	877.5	487.5	2.14	24.30	.865
	2		24.0	61.0	18.9	48.0	6.01					1.99	22.59	.834
	3		---	---	---	---	---	----	----	----	----	---	----	---
	1	621	12.0	30.5	6.9	17.5	5.98	522.6	3.603	875.5	486.4	1.97	22.36	.810
	2		24.0	61.0	18.9	48.0	6.01					1.99	22.59	.842
	3		---	---	---	---	---	----	----	----	----	---	----	---
	1	622	12.0	30.5	6.9	17.5	5.98	521.8	3.598	874.9	486.1	2.08	23.61	.824
	2		24.0	61.0	18.9	48.0	6.01					1.99	22.59	.810
	3		---	---	---	---	---	----	----	----	----	---	----	---
	1	623	12.0	30.5	6.9	17.5	5.98	521.5	3.596	875.3	486.3	2.11	23.95	.843
	2		24.0	61.0	18.9	48.0	6.01					1.99	22.59	.815
	3		---	---	---	---	---	----	----	----	----	---	----	---

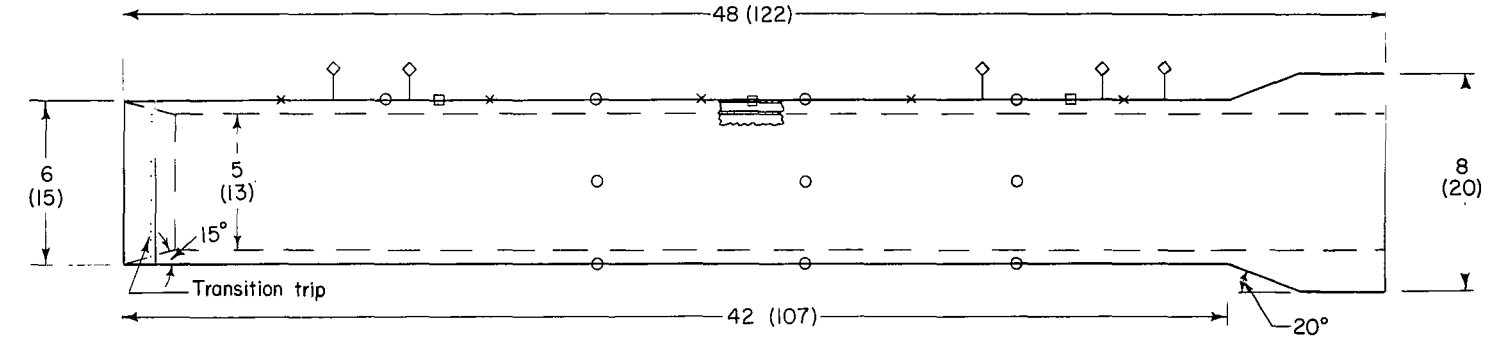

		Locations
×	Thermocouples	6(15), 14(36), 22(56), 30(76), 38(96)
□	Heat flowmeters	12(30), 24(61), 36(91)
○	Static orifices	10(25), 18(46), 26(66), 34(86)
◇	Stations	8(20), 11(28), 33(84), 37(94), 40(102)

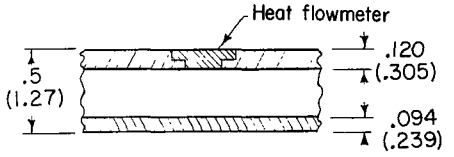

Enlarged cross section of wall heat flowmeter

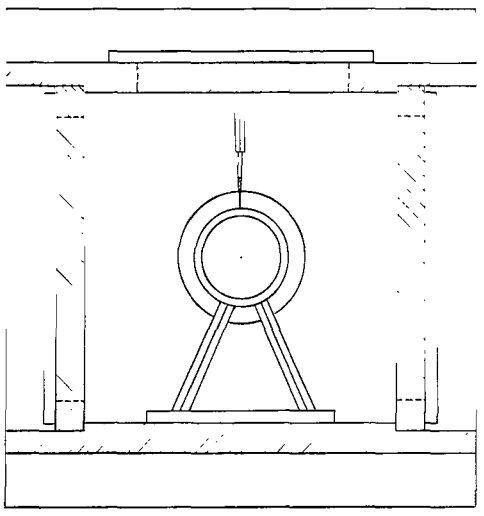

Front view
(mounted in tunnel)

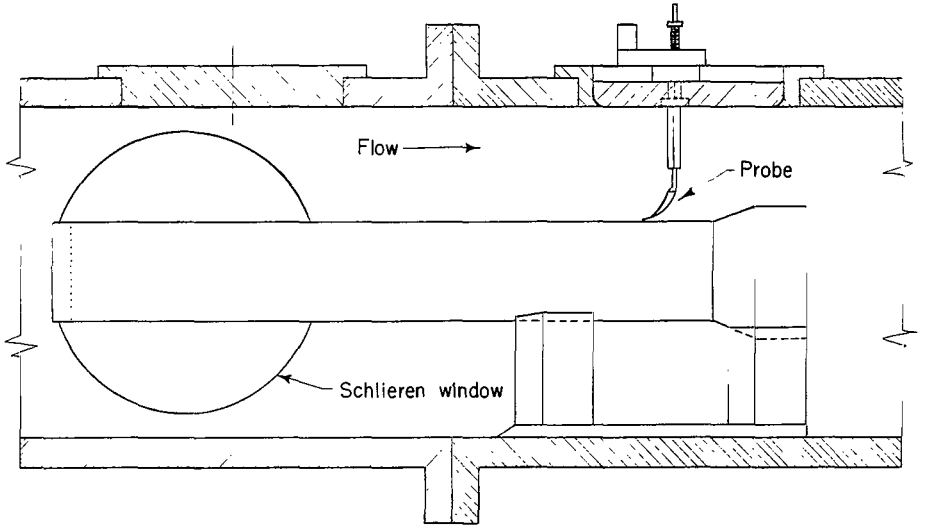

Side view
(mounted in tunnel)

Figure 1.- Cylinder model with dimensions and probe instrumentation. All dimensions are in inches, centimeters in parentheses.

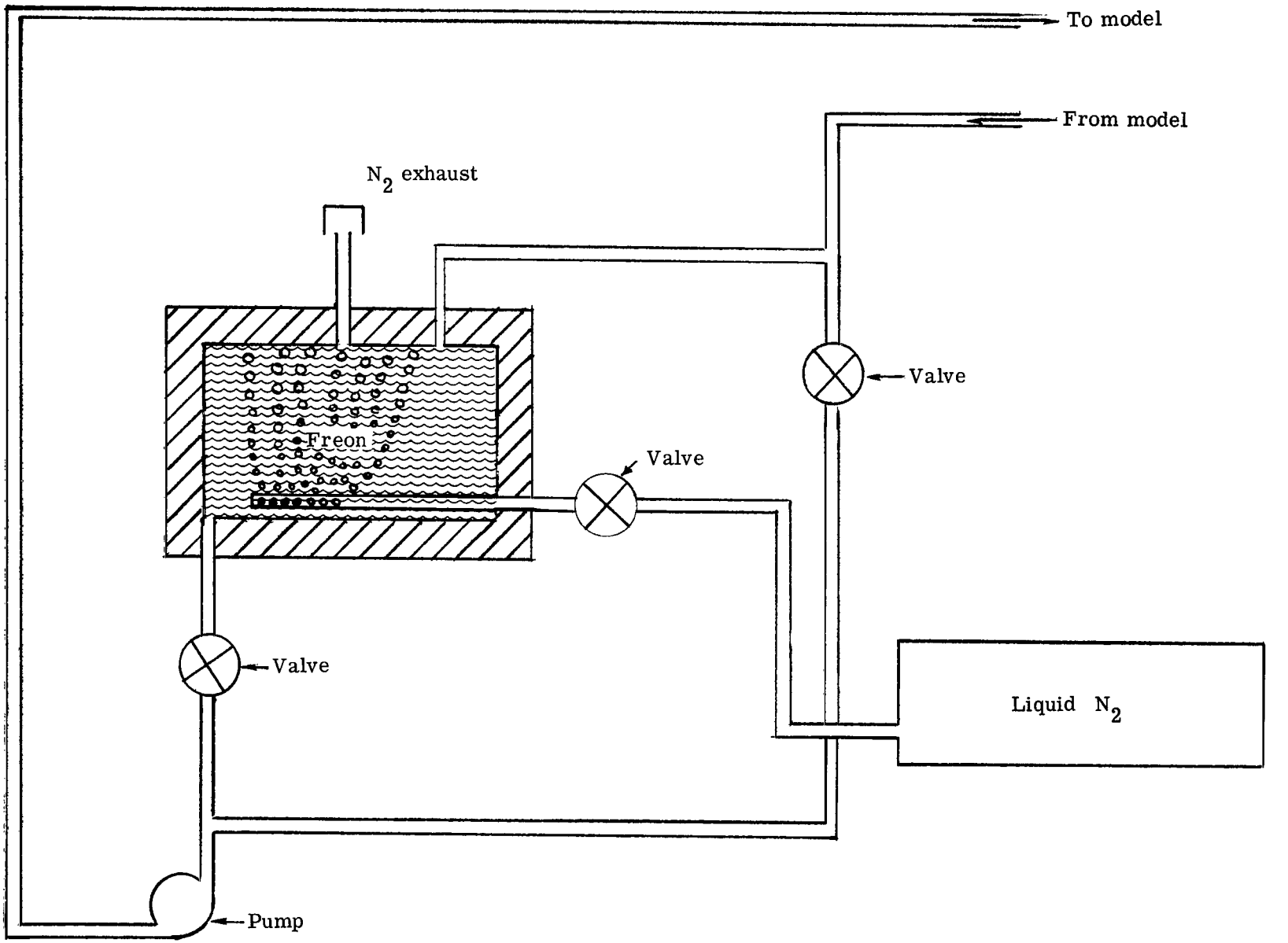

Figure 2.- Diagram of cooling system.

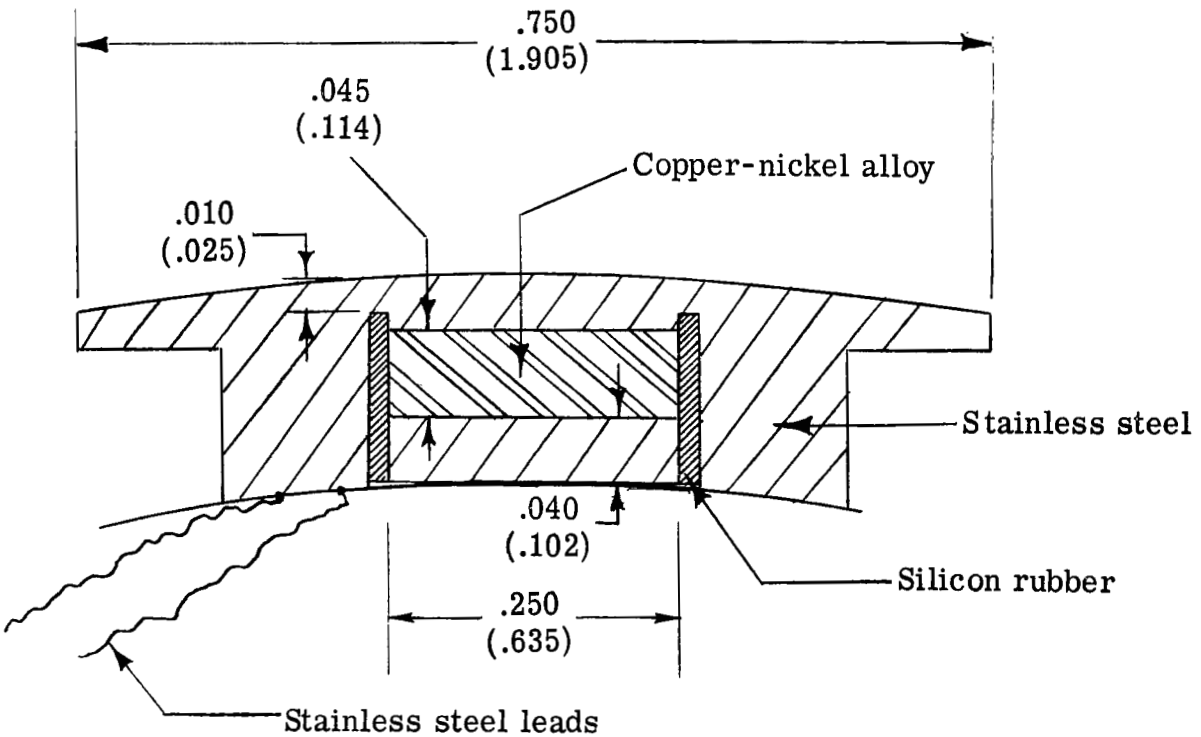

Figure 3.- Cross-sectional view of heat flowmeter. All dimensions are in inches, centimeters in parentheses.

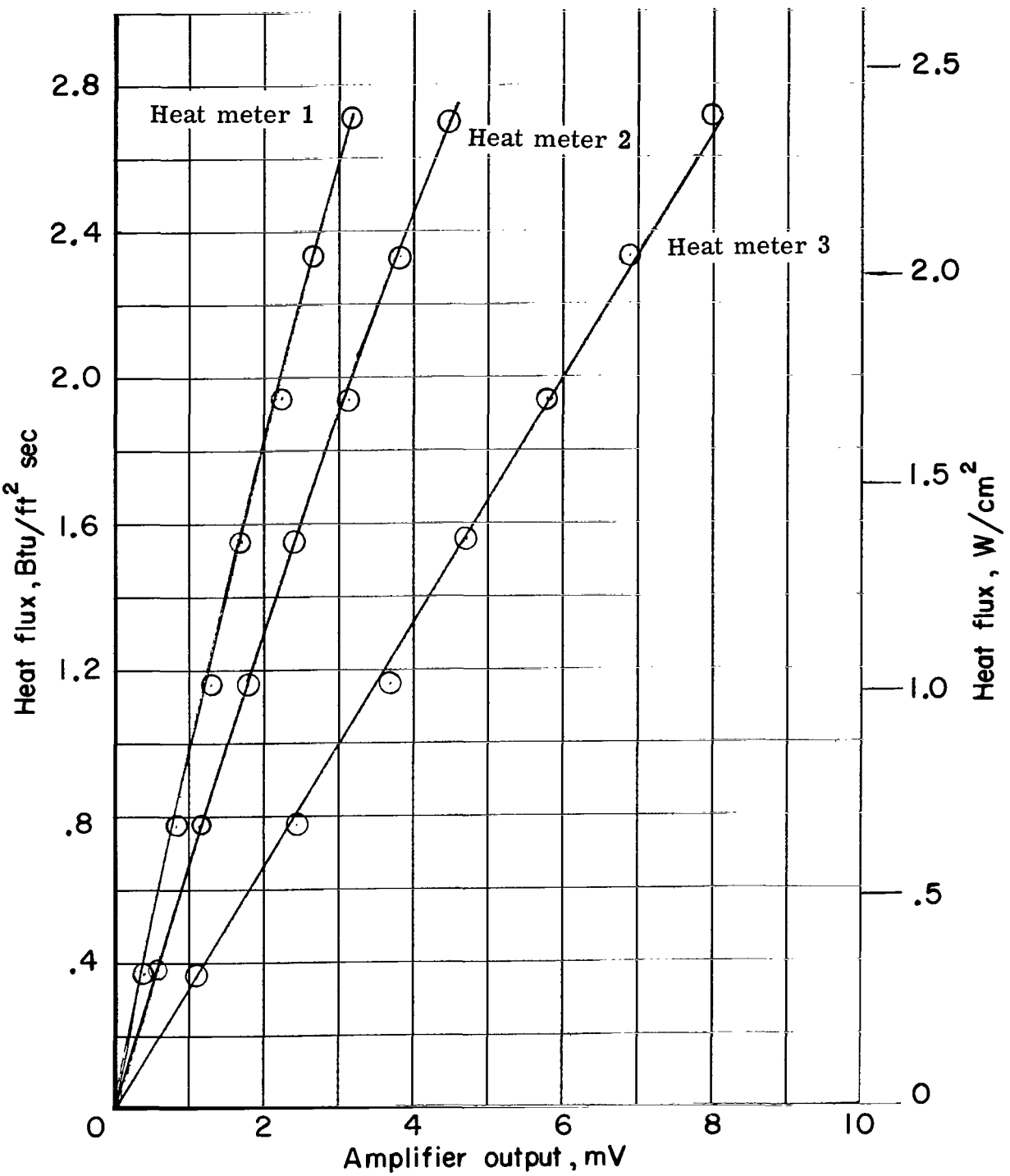

Figure 4.- Calibration of heat flowmeters. Coolant temperature = -100° F (-73° C).

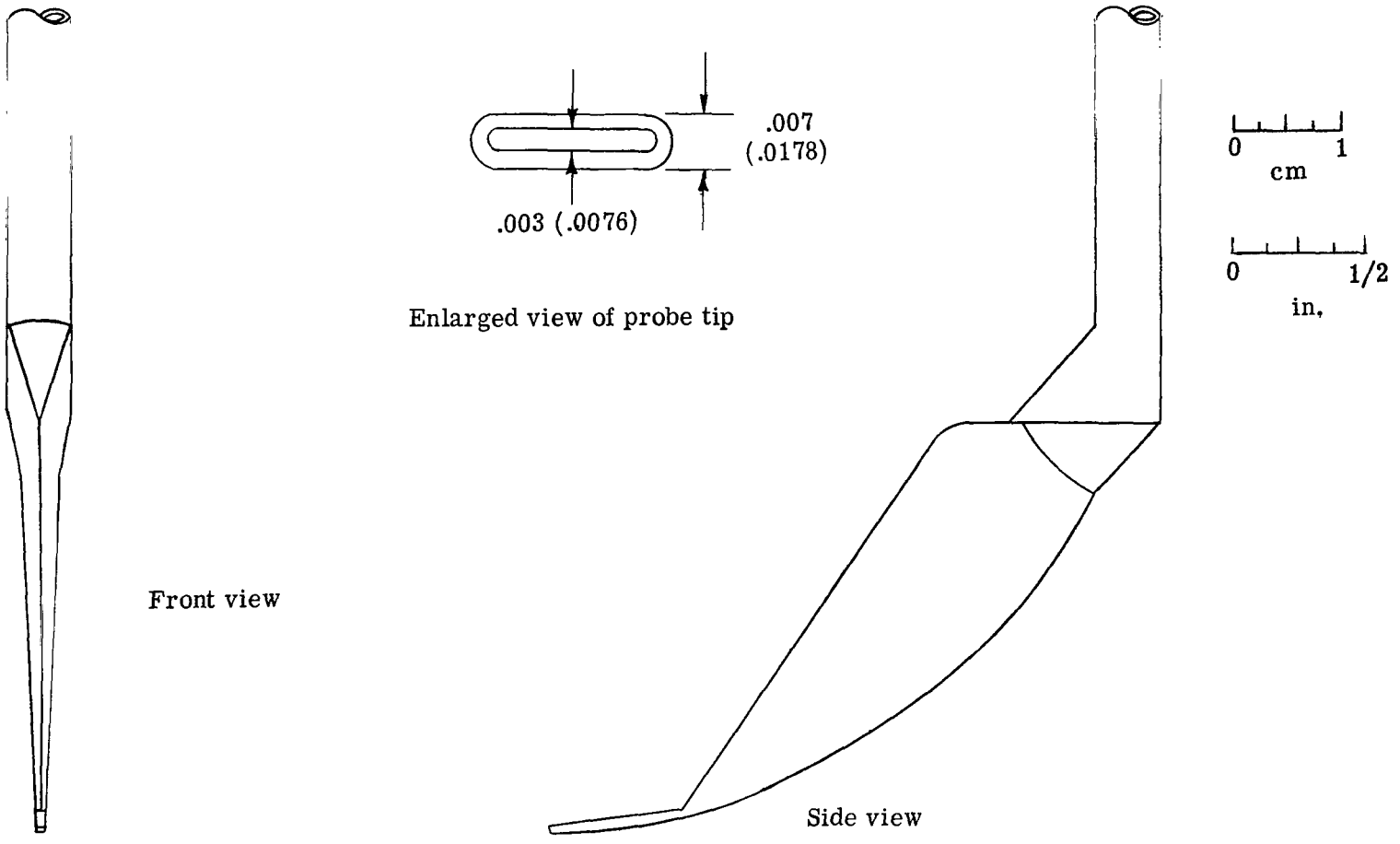

Figure 5.- Schematic of boundary-layer pressure probe. All dimensions are in inches, centimeters in parentheses.

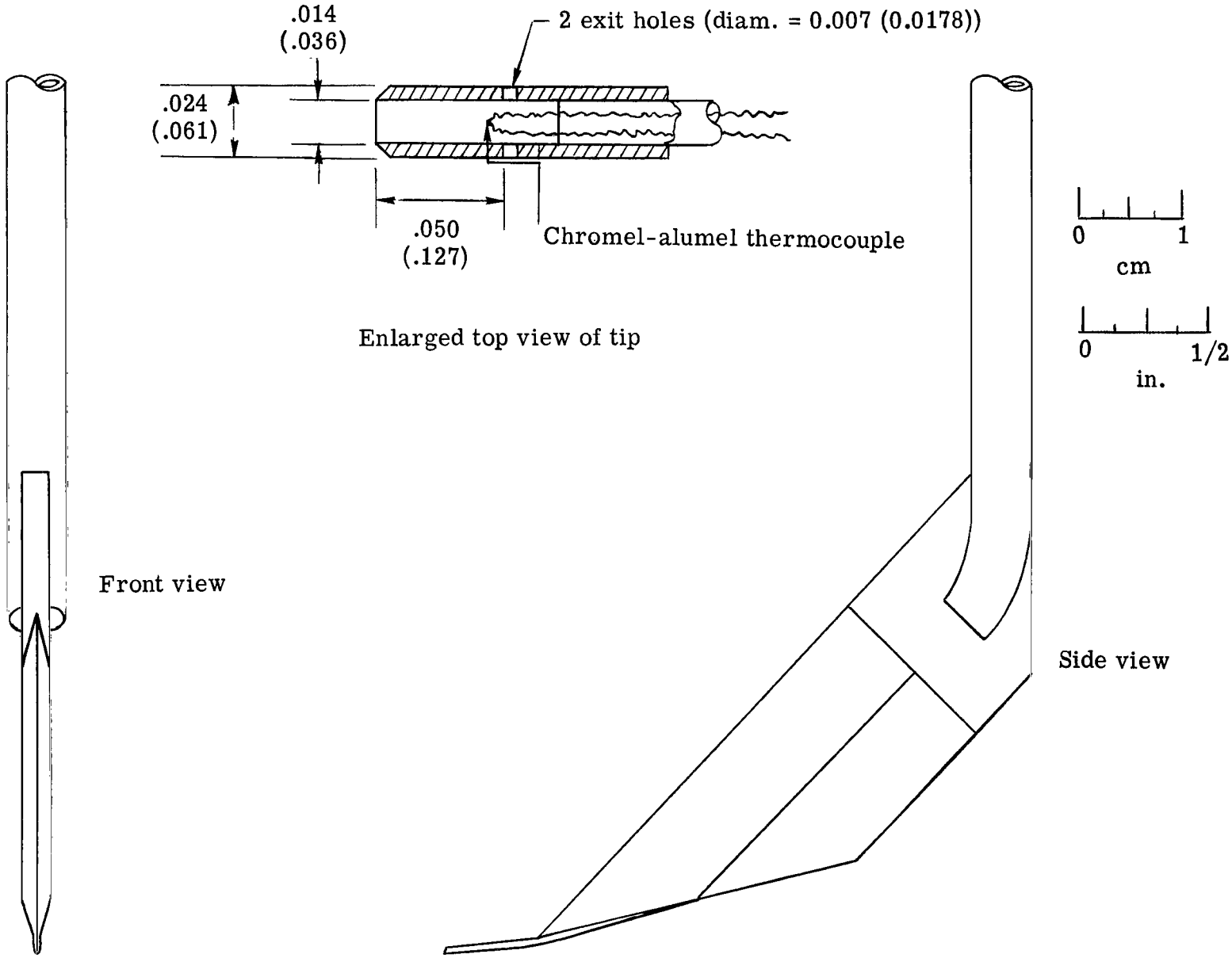

Figure 6.- Schematic of boundary-layer temperature probe. All dimensions are in inches, centimeters in parentheses.

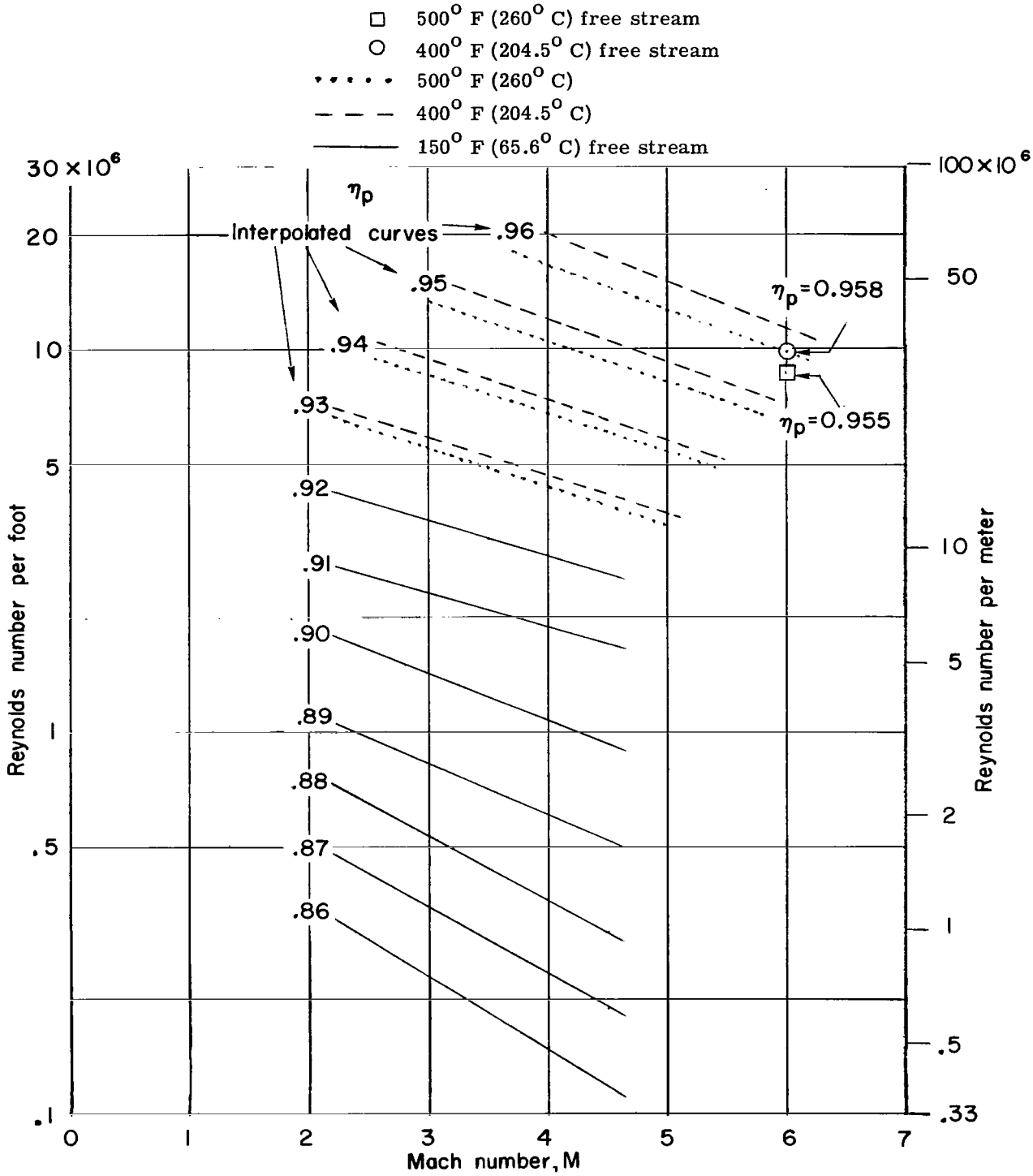

Figure 7.- Calibration plot of boundary-layer temperature probe.

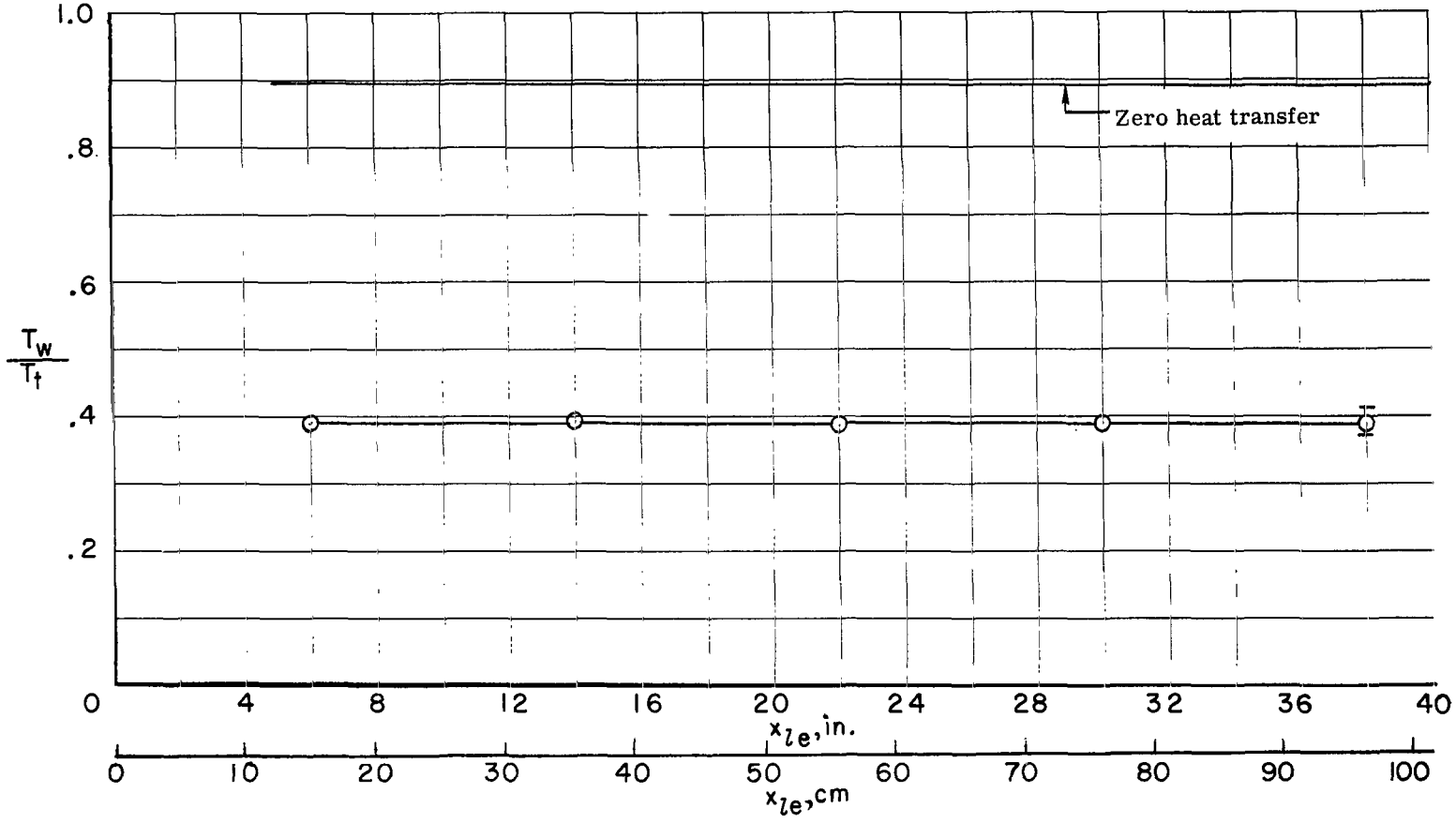

(a) $T_w/T_{aw} = 0.44$.

Figure 8.- Variation of wall temperature with distance from leading edge.

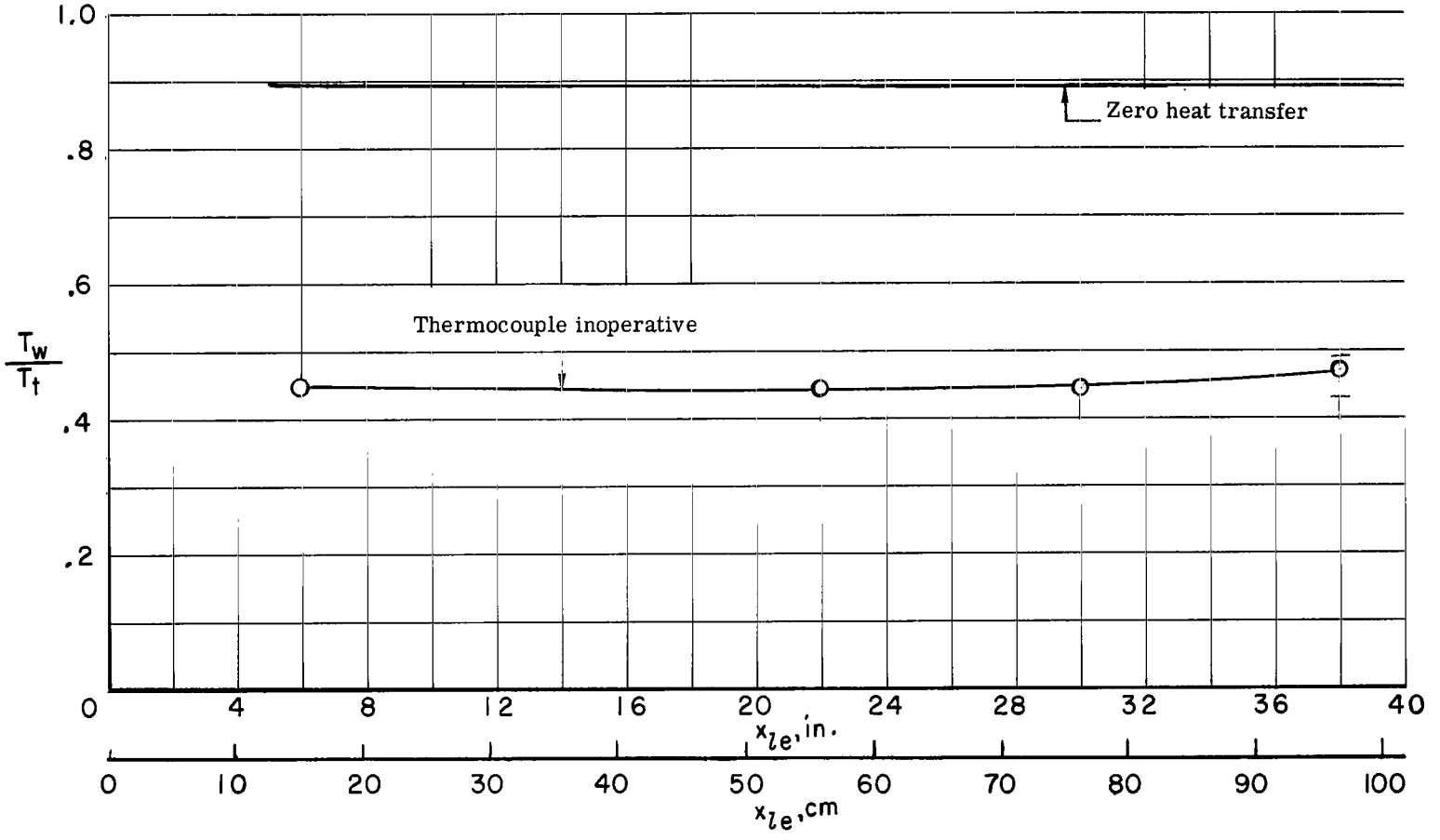

(b) $T_w/T_{aw} = 0.50$.

Figure 8.- Concluded.

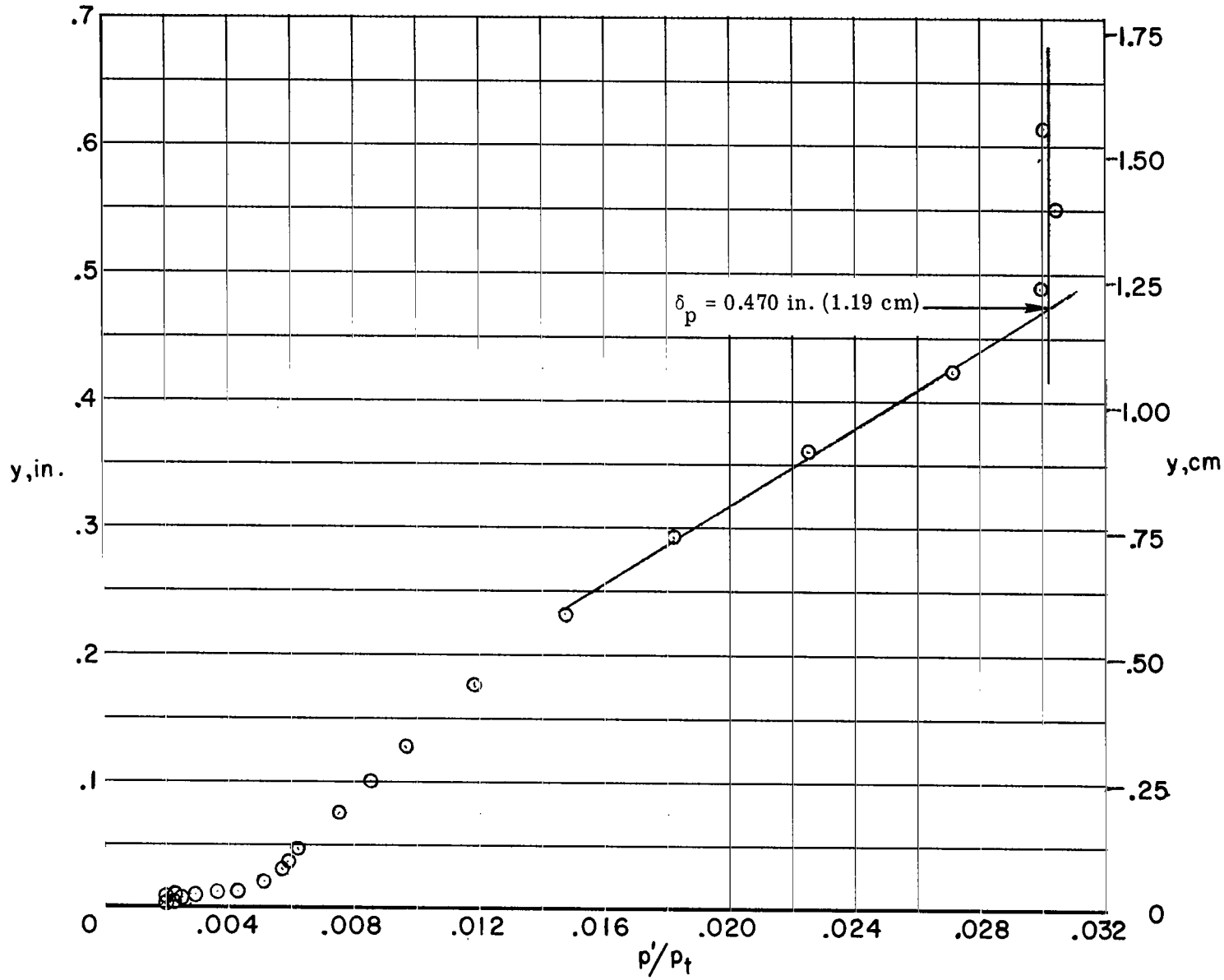

Figure 9.- Typical pitot-pressure distribution through boundary layer. (Distribution shown is for station 4, T_w/T_{aw} = 0.50.)

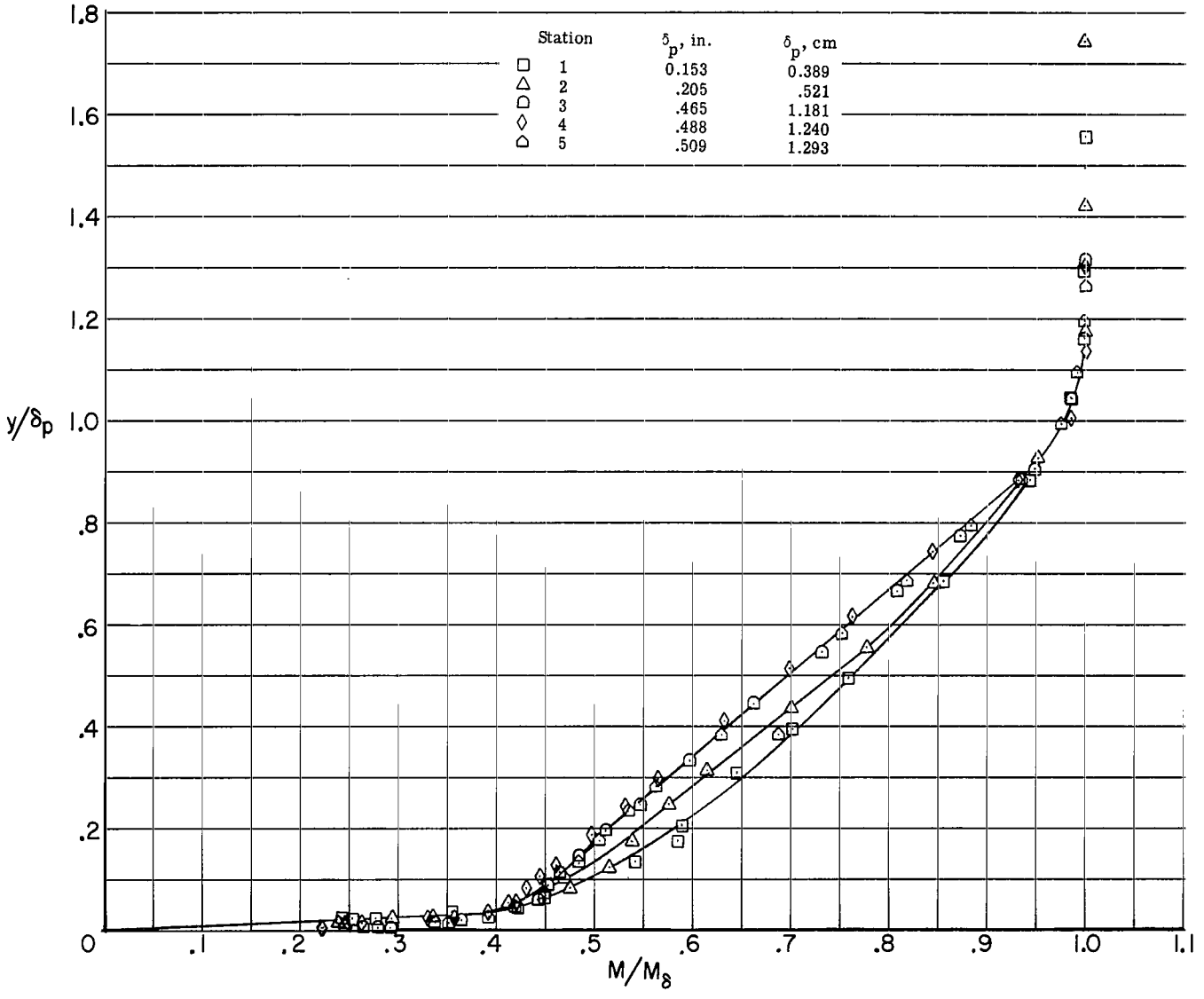

(a) $T_w/T_{aw} = 0.44$.

Figure 10.- Boundary-layer Mach number profiles.

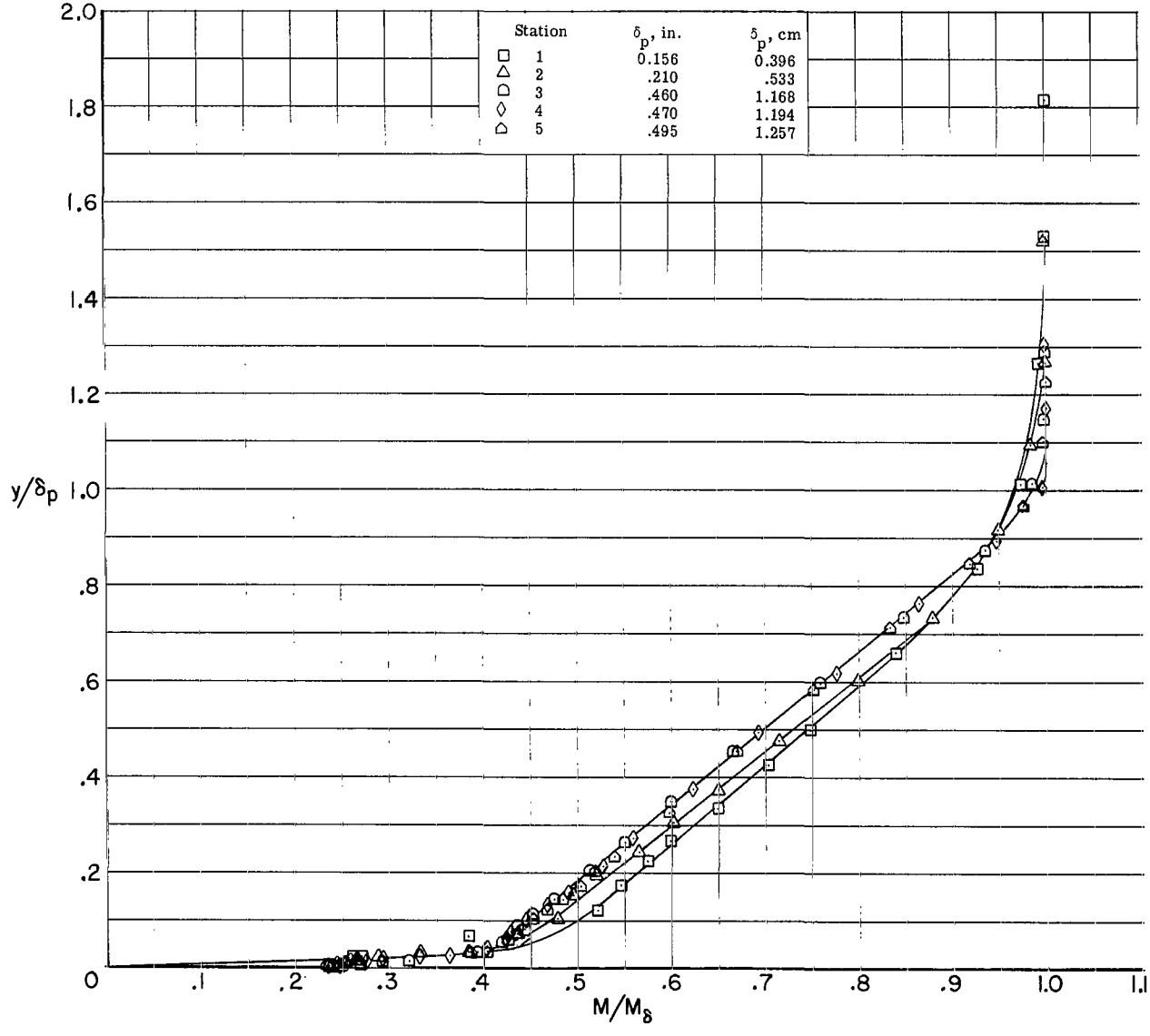

(b) $T_w/T_{aw} = 0.50$.

Figure 10.- Concluded.

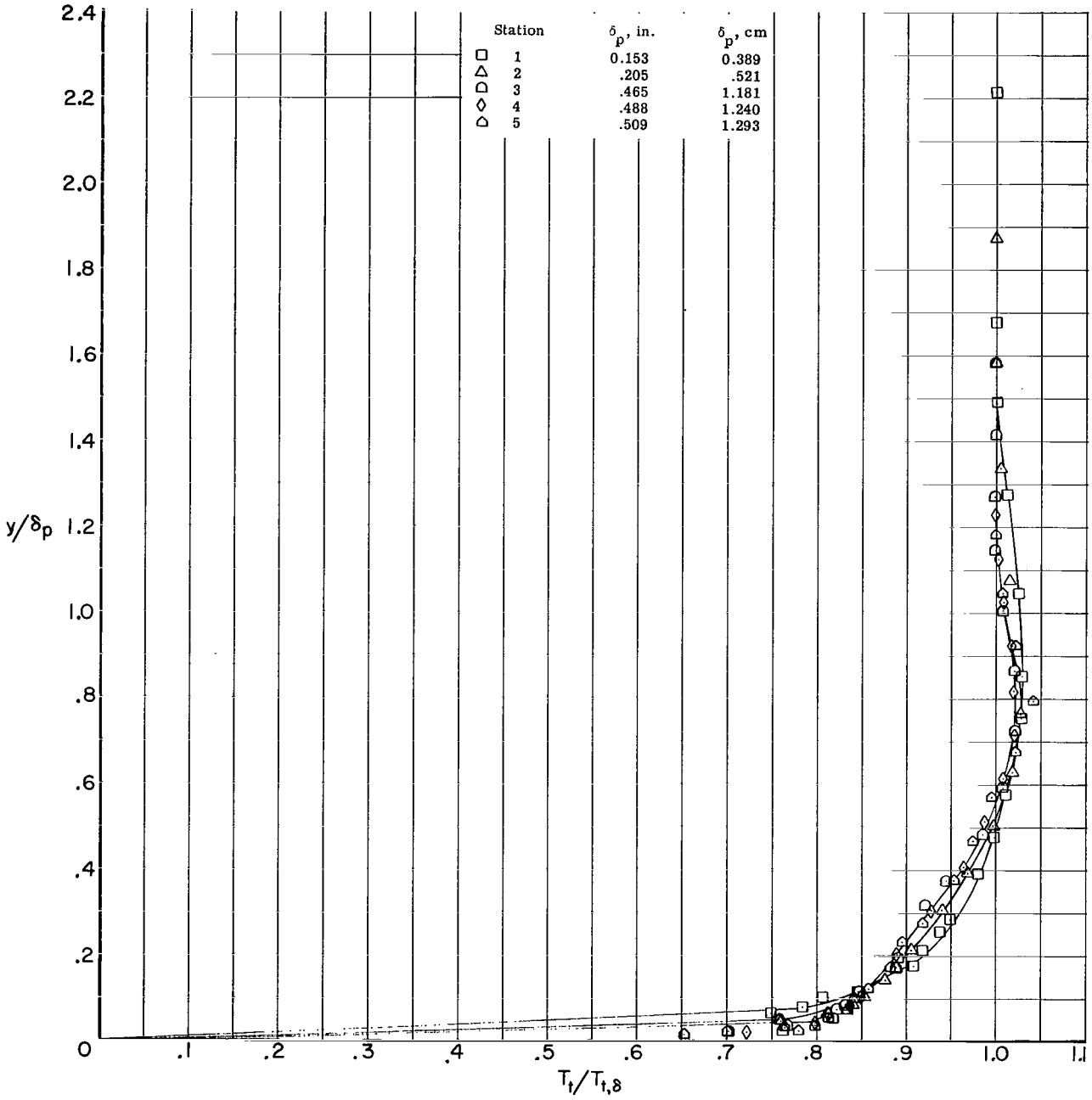

(a) T_w/T_{aw} = 0.44.

Figure 11.- Boundary-layer total-temperature profiles.

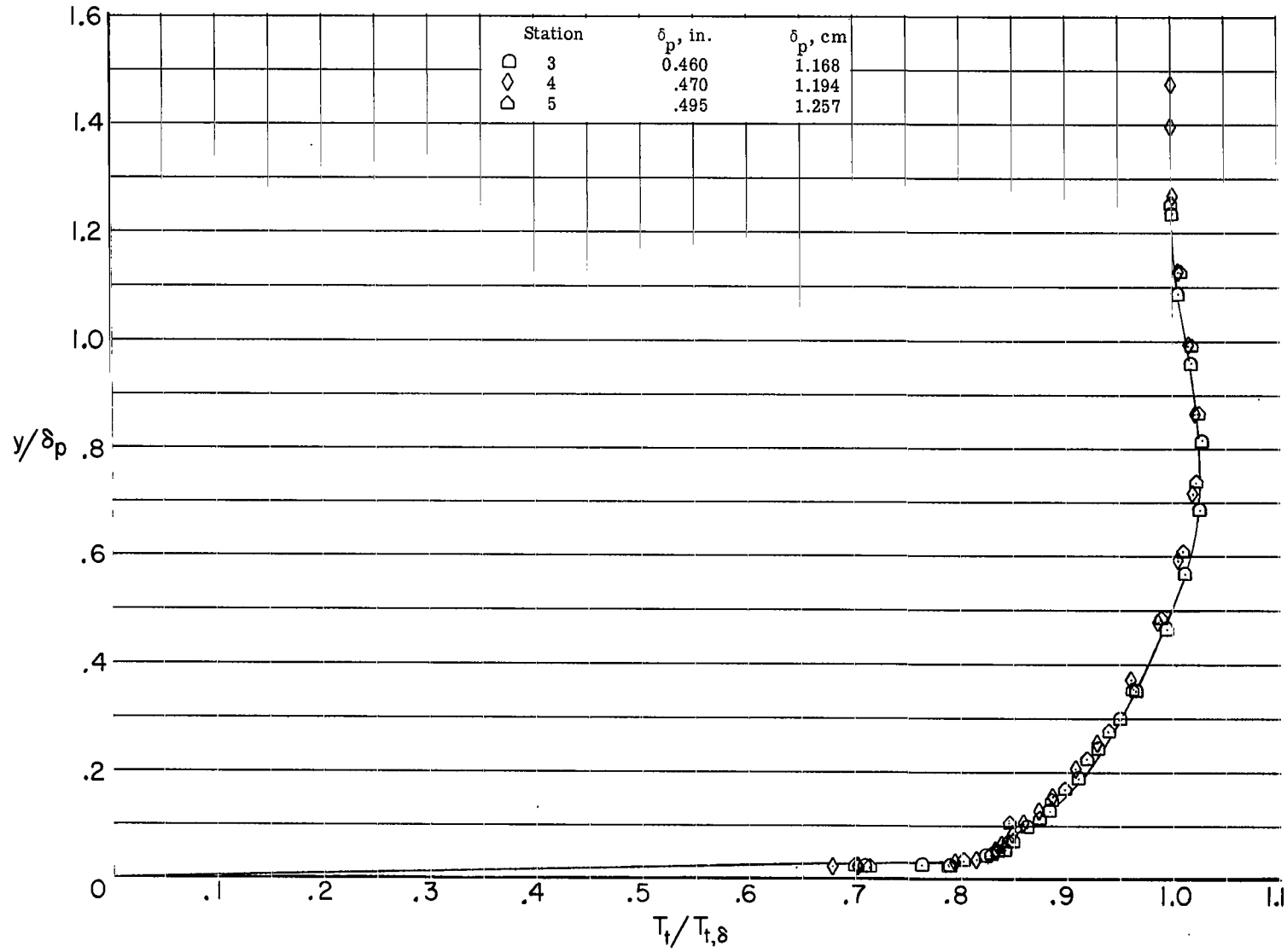

(b) $T_w/T_{aw} = 0.50$.

Figure 11.- Concluded.

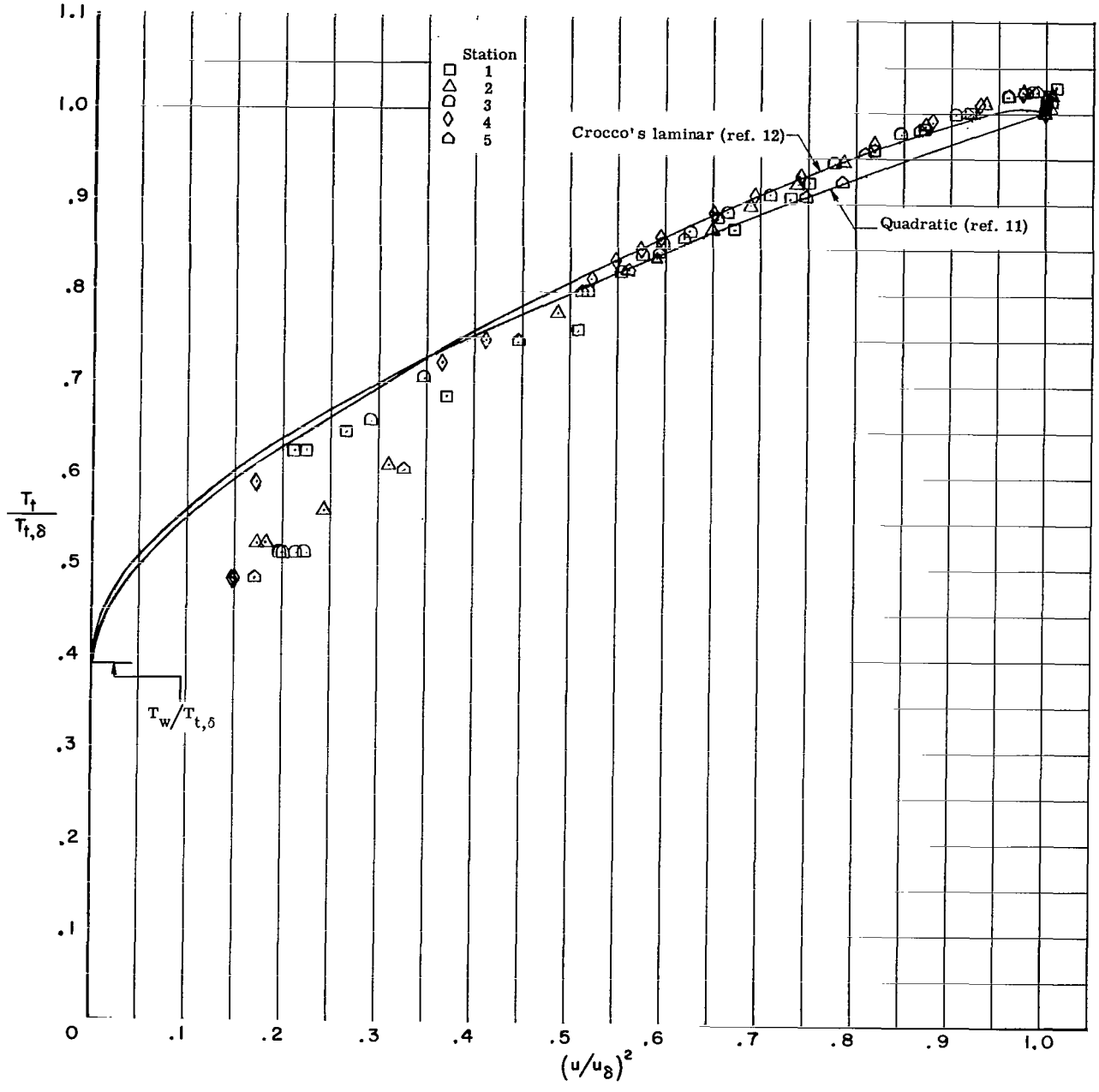

(a) $T_w/T_{aw} = 0.44$.

Figure 12.- Comparison of theoretical and measured variation of boundary-layer total-temperature ratio with velocity ratio squared.

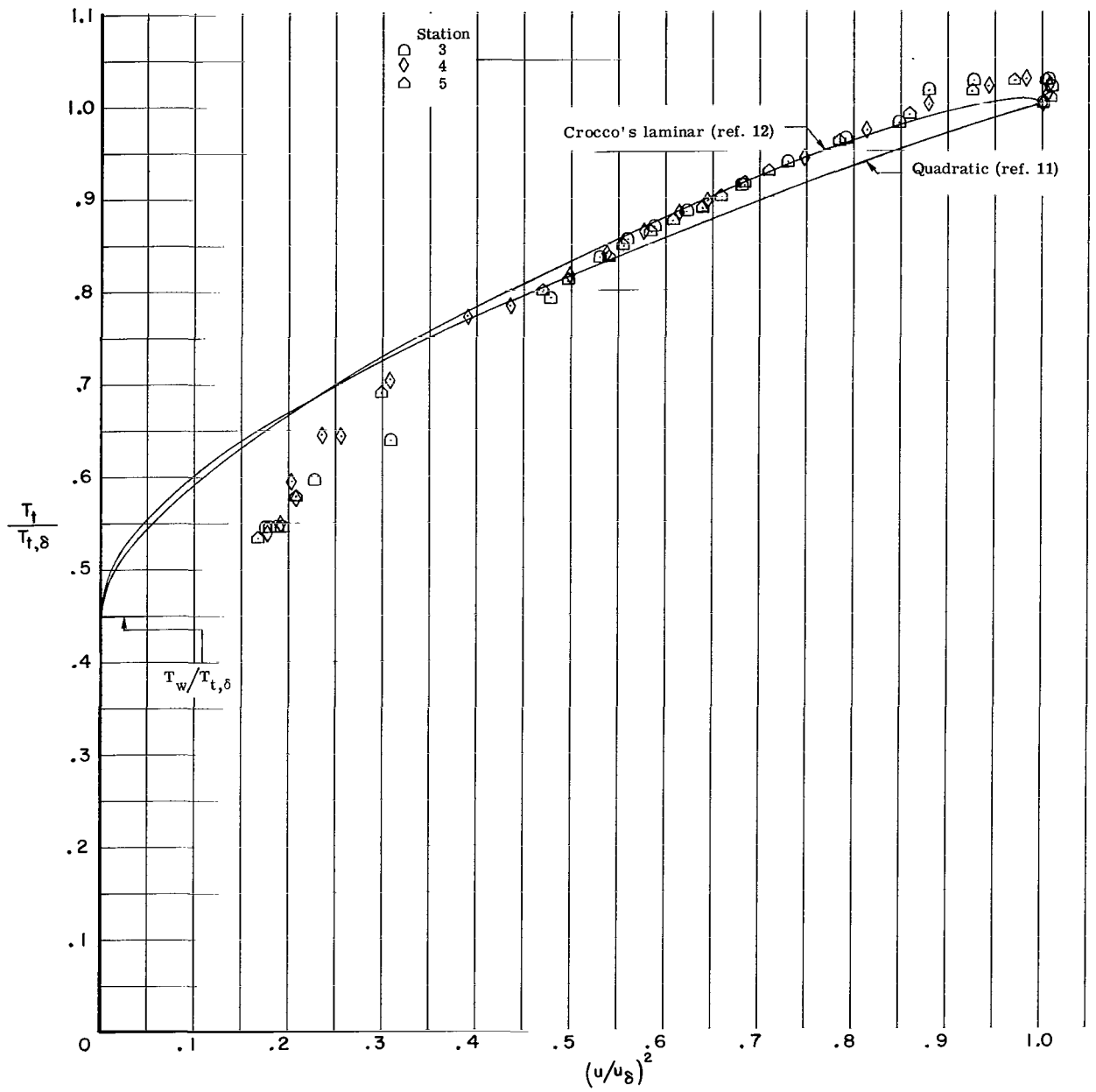

(b) $T_w/T_{aw} = 0.50$.

Figure 12.- Concluded.

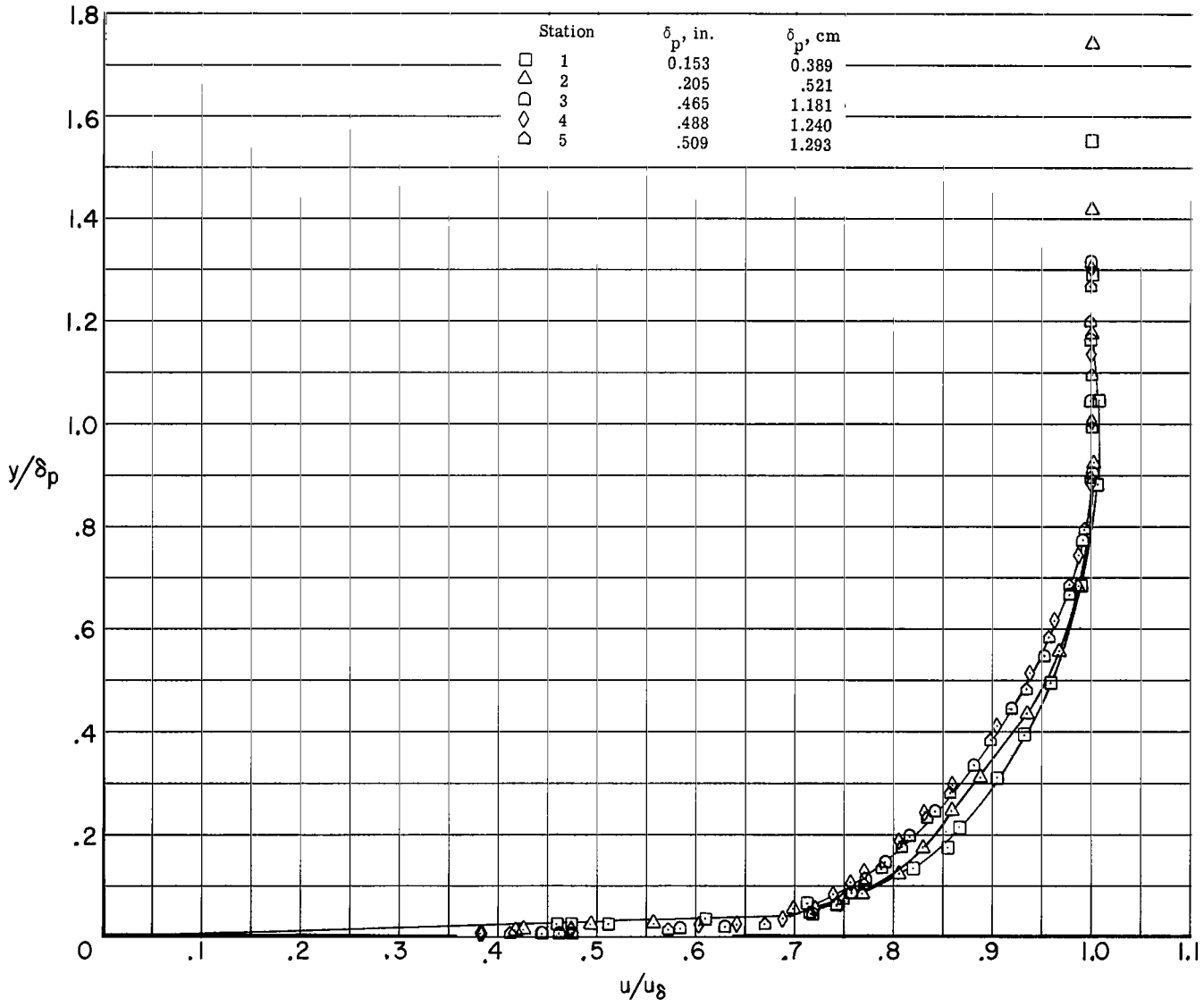

(a) T_w/T_{aw} = 0.44.

Figure 13.- Boundary-layer velocity profiles.

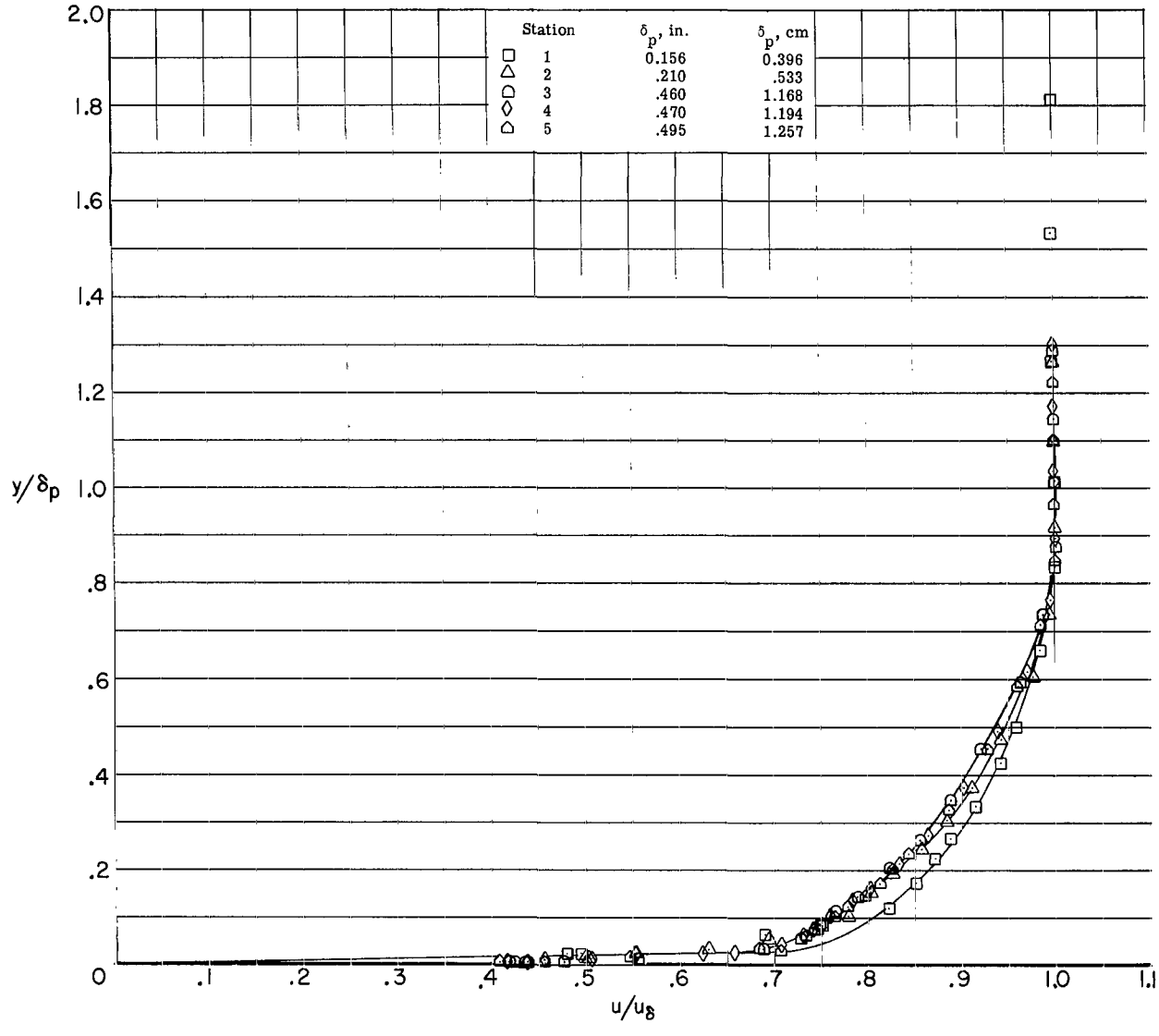

(b) $T_w/T_{aw} = 0.50$.

Figure 13.- Concluded.

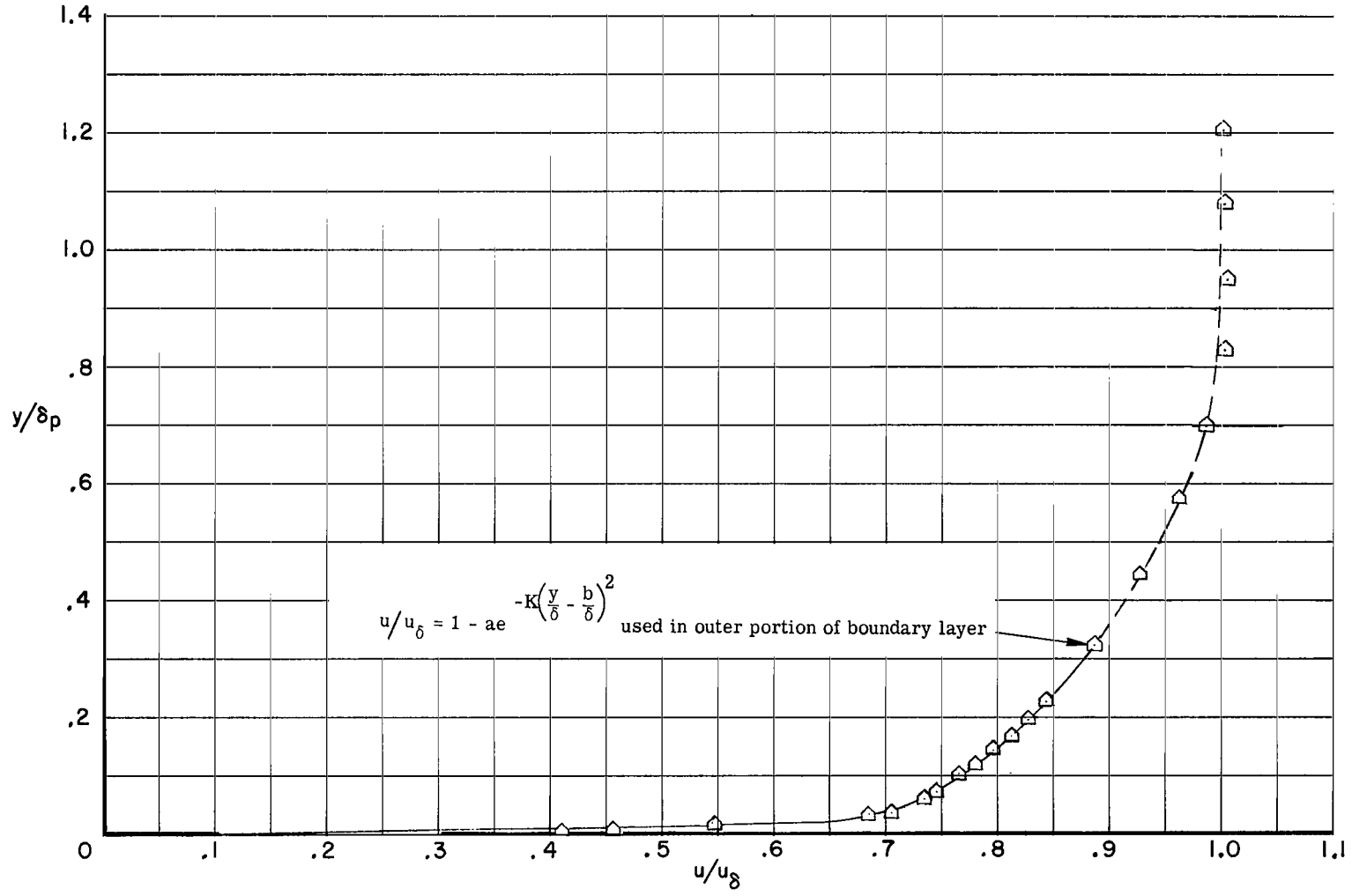

Figure 14.- Comparison of measured velocity profiles with exponentially calculated profiles.

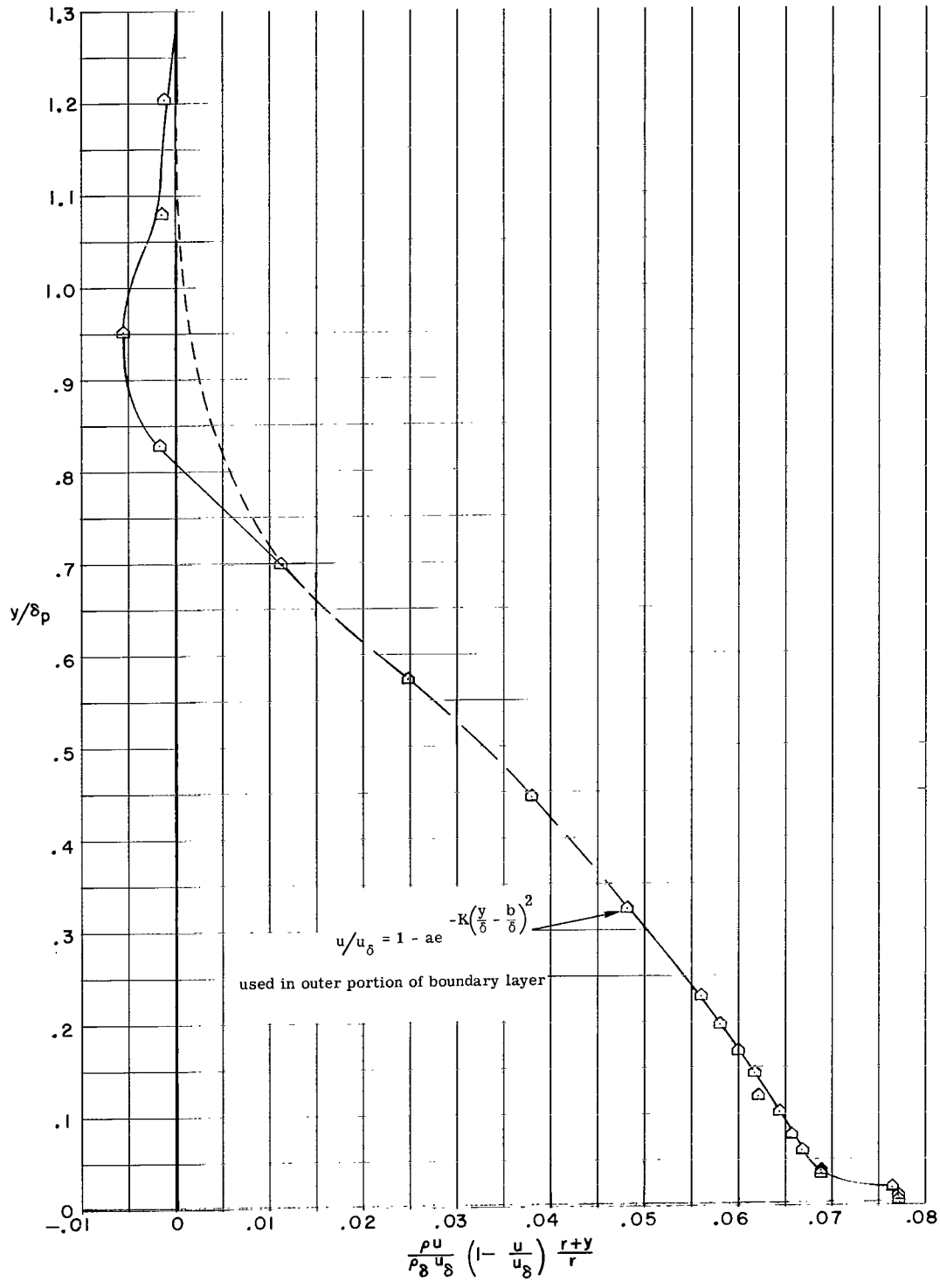

Figure 15.- Comparison of measured momentum thickness profile with exponentially calculated profile.

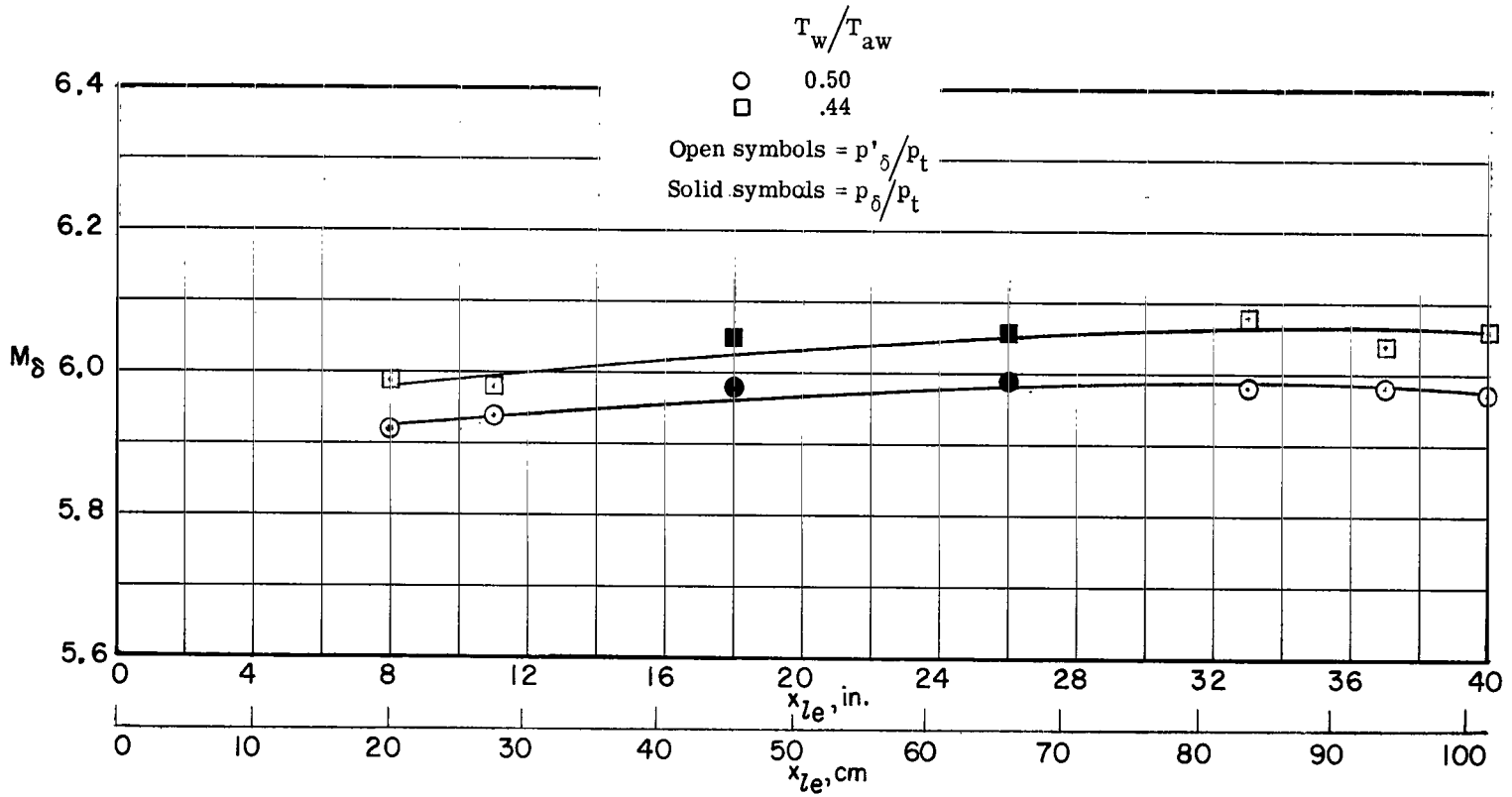

Figure 16.- Longitudinal Mach number distribution on the cylinder.

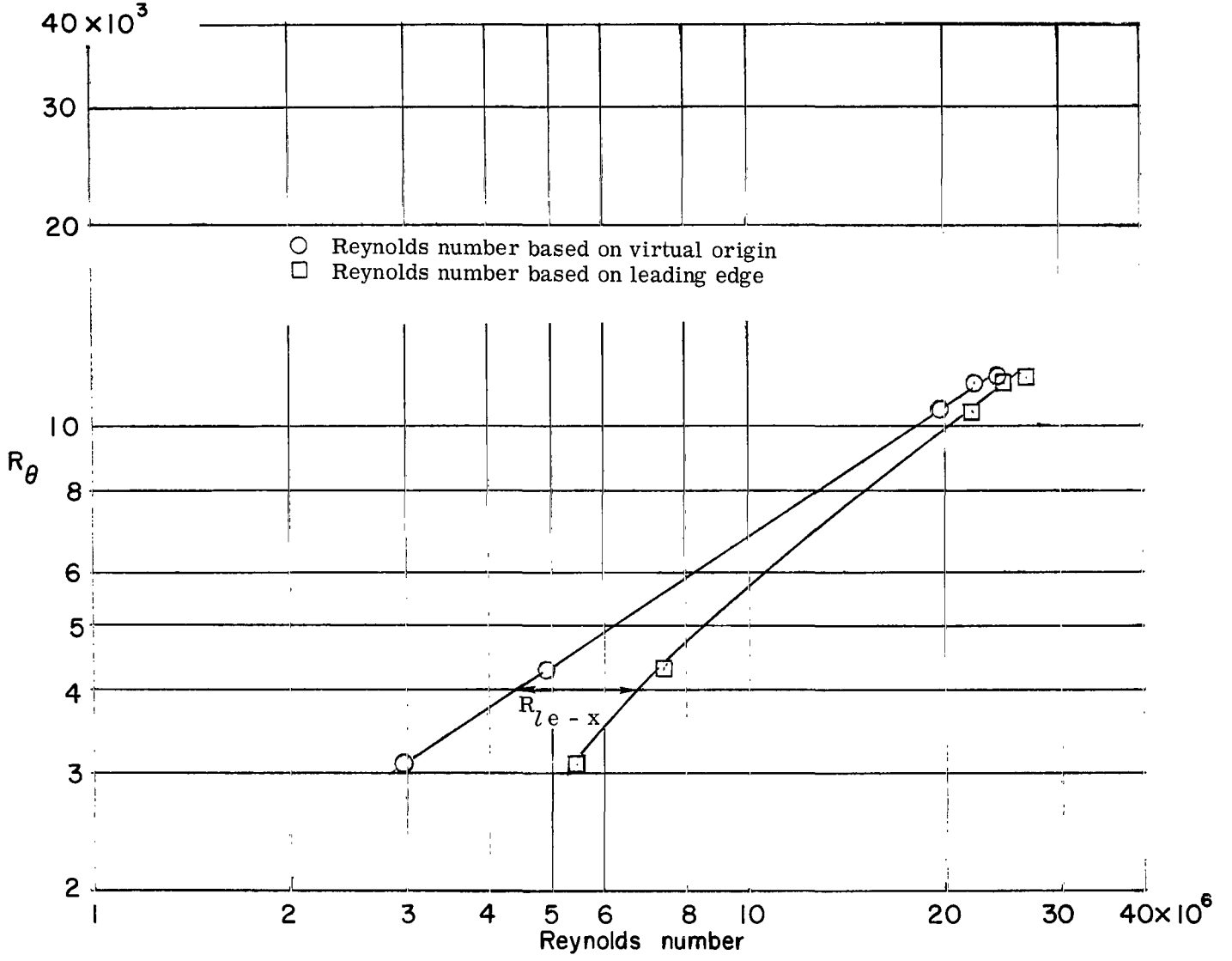

(a) $T_w/T_{aw} = 0.44$.

Figure 17.- Variation of Reynolds number based on momentum thickness with Reynolds number.

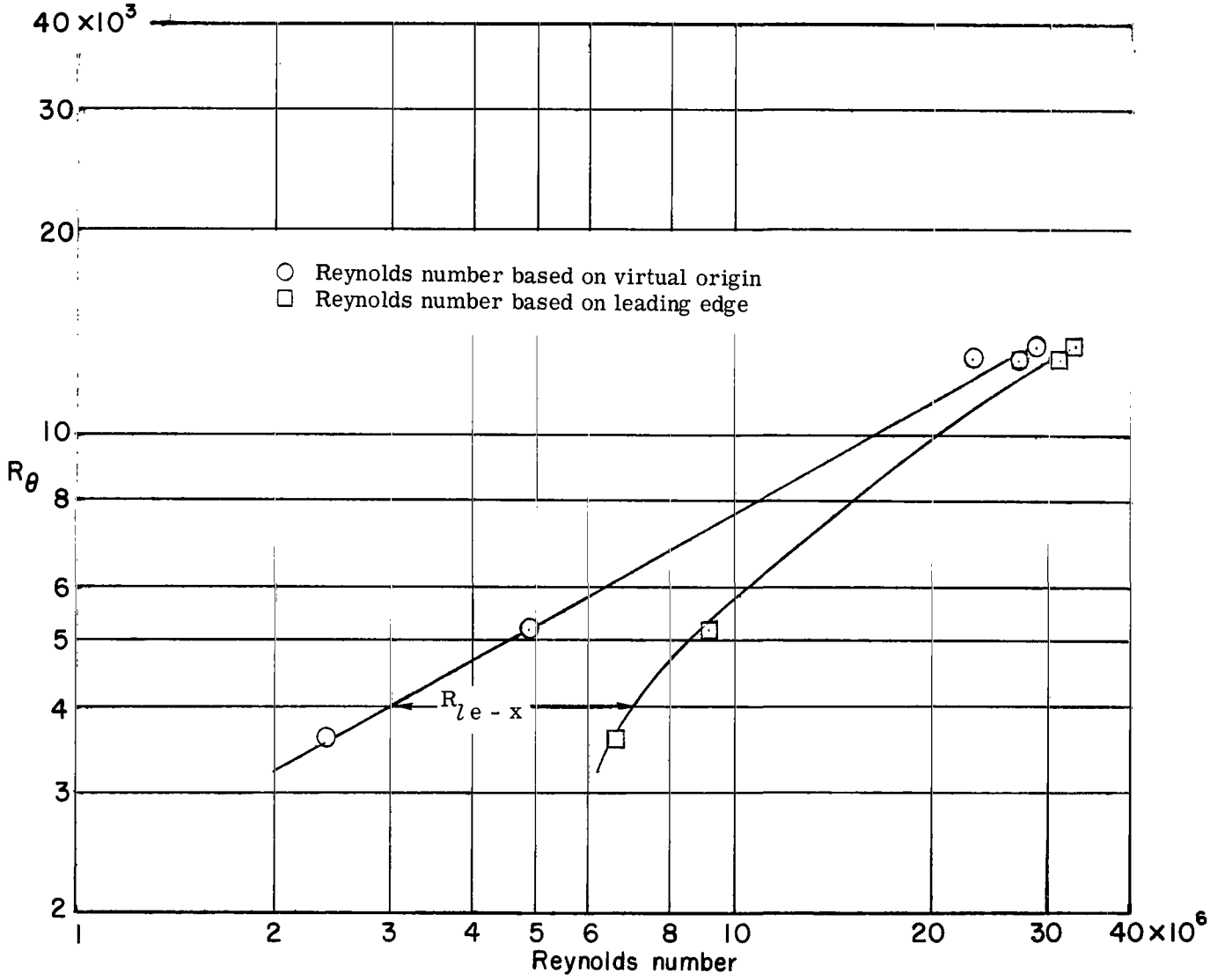

(b) $T_w/T_{aw} = 0.50$.

Figure 17.- Concluded.

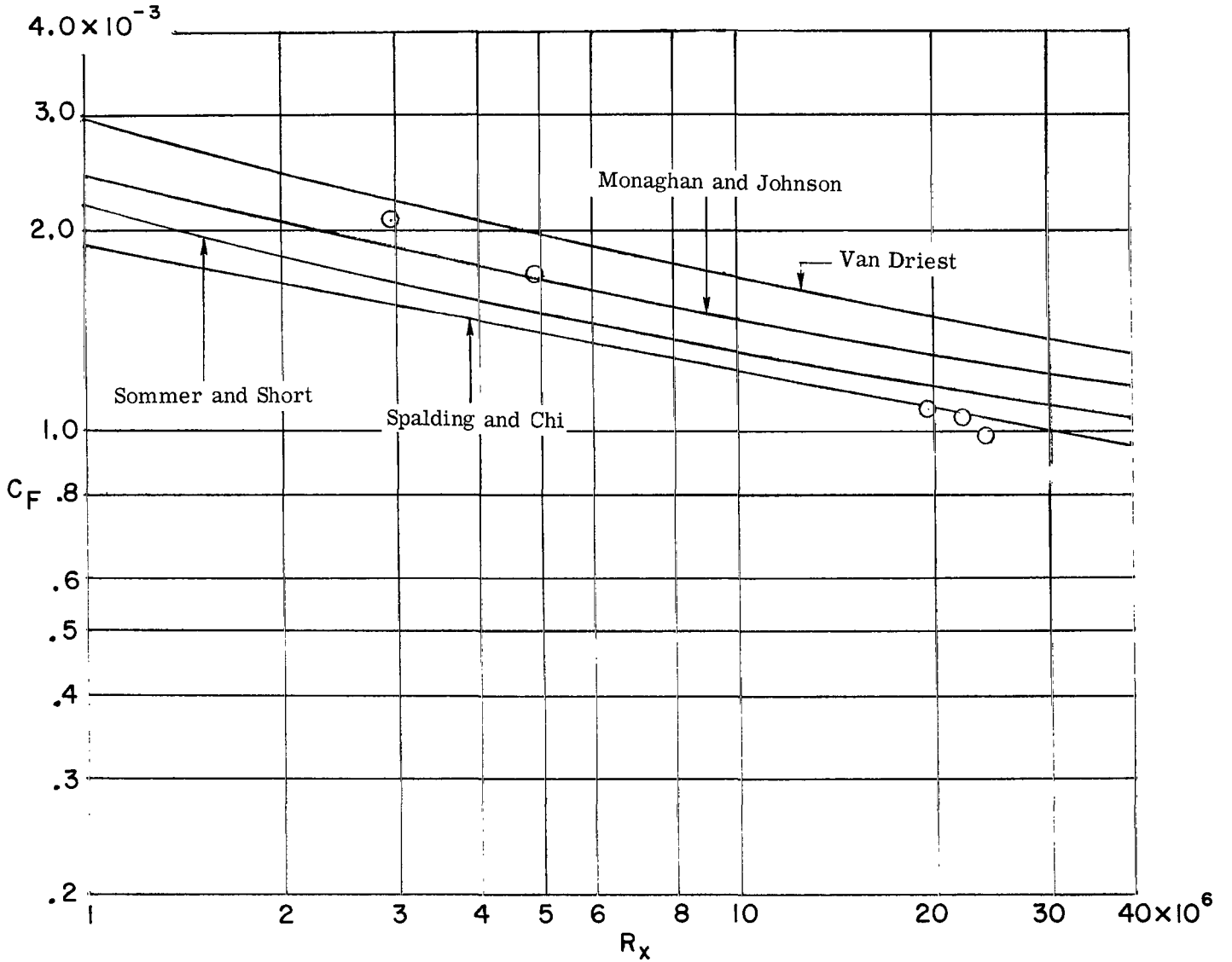

(a) $T_w/T_{aw} = 0.44$.

Figure 18.- Variation of average skin-friction coefficient with effective Reynolds number.

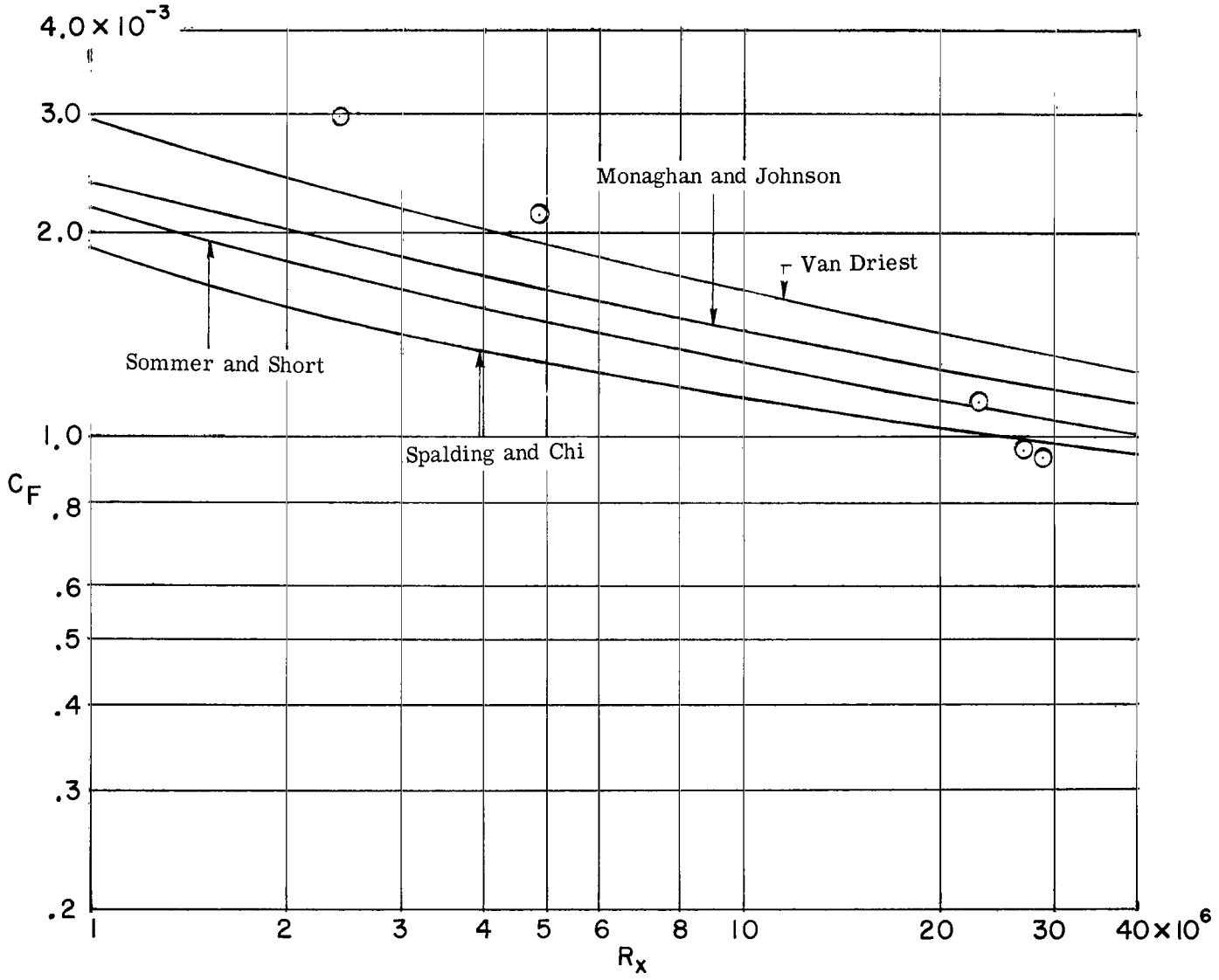

(b) $T_w/T_{aw} = 0.50$.

Figure 18.- Concluded.

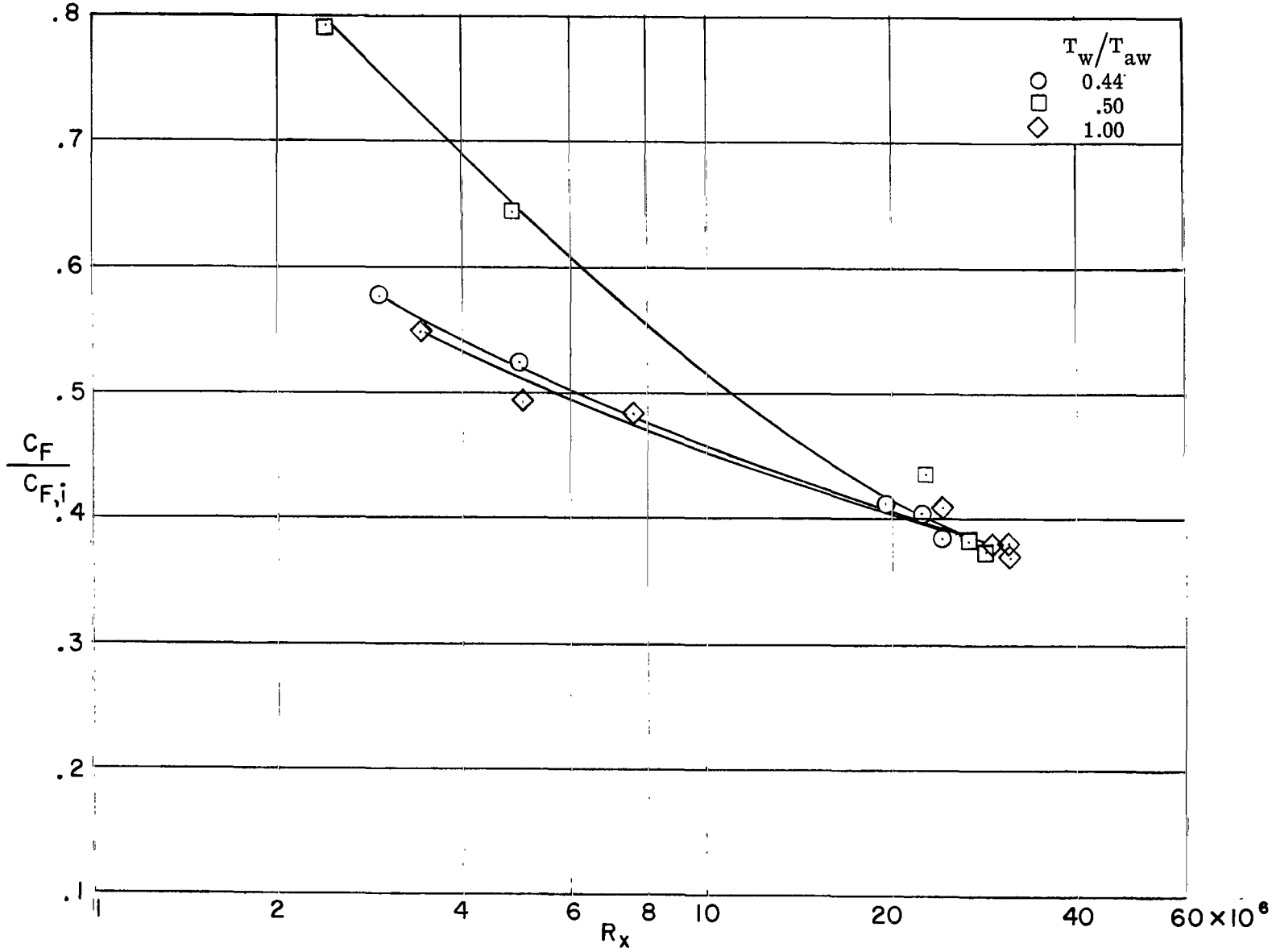

Figure 19.- Variation of ratio of average skin friction to incompressible skin friction with effective Reynolds number at various wall-temperature ratios.

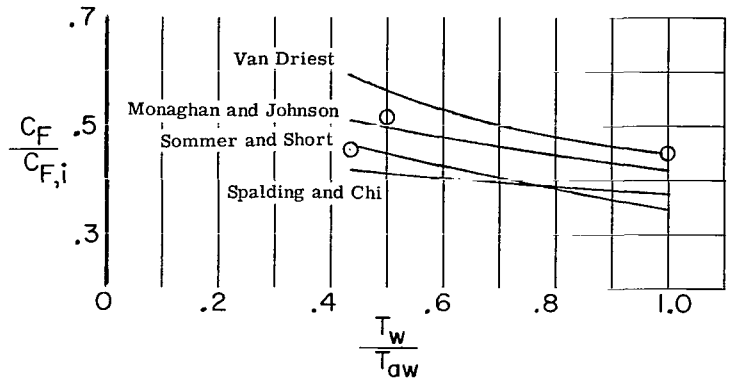

(a) $R_x = 10 \times 10^6$.

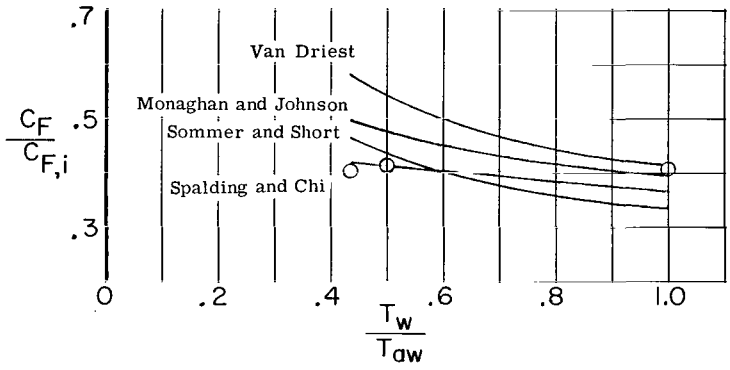

(b) $R_x = 20 \times 10^6$.

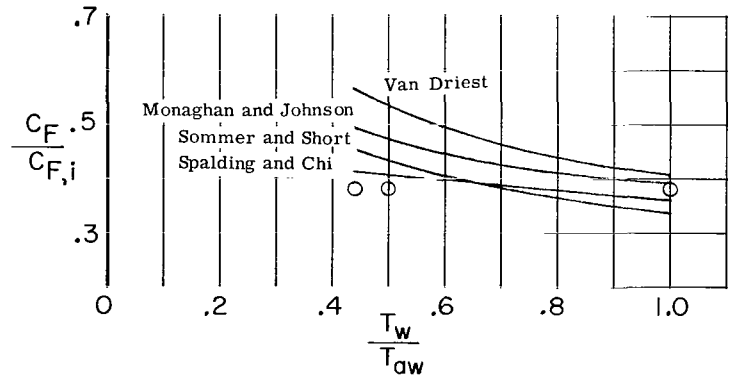

(c) $R_x = 30 \times 10^6$.

Figure 20.- Variation of ratio of average skin friction to incompressible skin friction with wall-temperature ratio at various effective Reynolds numbers. Points shown were obtained from cross plot of figure 19. Adiabatic data taken from reference 1.

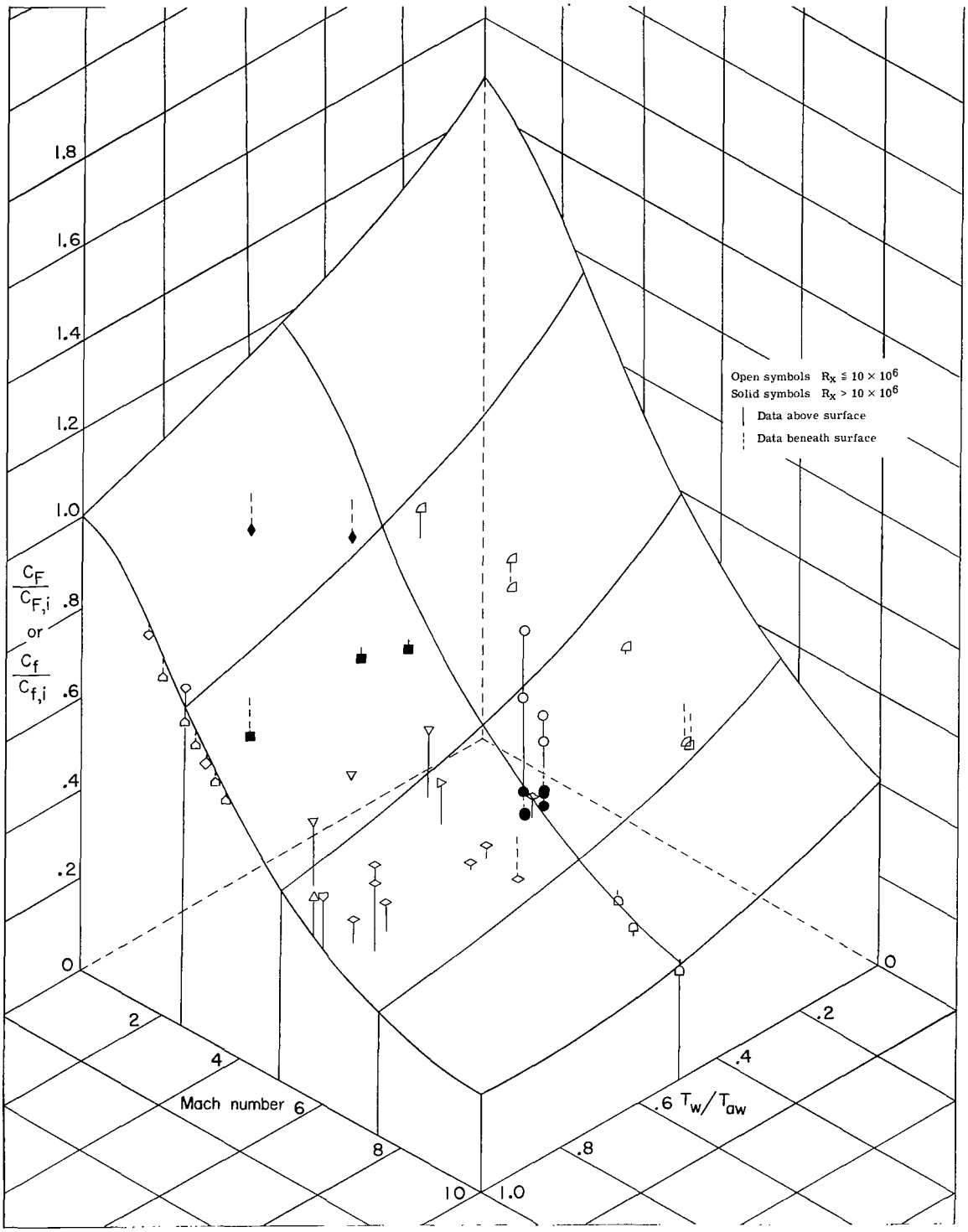

Figure 21.- Variation of various experimental skin-friction coefficients with Mach number and wall-temperature ratio at various Reynolds numbers. Surface as determined from Sommer and Short T' theory for $R_x = 10 \times 10^6$.

KEY FOR FIGURE 21

Author	Mach number	T_w / T_{aw}	Reynolds number
○ Present data	6.00	0.44 to 0.50	2.4×10^6 to 28.7×10^6
□ Swanson, et al. (ref. 17)	2.89 to 3.53	0.54 to 0.87	47.0×10^6 to 100.0×10^6
△ Korkegi (ref. 18)	5.80	1.00	10×10^6
◇ Brinich and Diaconis (ref. 19)	3.05	1.00	10×10^6
Sommer and Short (ref. 4)	2.81 to 7.00	0.18 to 0.43	1.6×10^6 to 5.2×10^6
Hill (ref. 20)	8.27 to 10.04	0.48 to 0.54	2.1×10^6 to 3.7×10^6
Maloney (ref. 22)	1.35 to 1.99	0.53 to 0.71	65.0×10^6 to 87.0×10^6
Wilson (ref. 14)	1.72 to 2.47	1.00	10×10^6
Chapman and Kester (ref. 16)	2.00 to 3.60	1.00	10×10^6
▽ Winkler and Cha (ref. 2)	5.14 to 5.25	0.65 to 0.94	3.0×10^6 to 4.6×10^6
Adcock, et al. (ref. 1)	6.00	1.00	10×10^6
◁▷ Danberg (ref. 3)	6.50	0.50 to 0.93	3.1×10^6 to 9.7×10^6
▷ Neal (ref. 21)	6.80	0.80	4.8×10^6

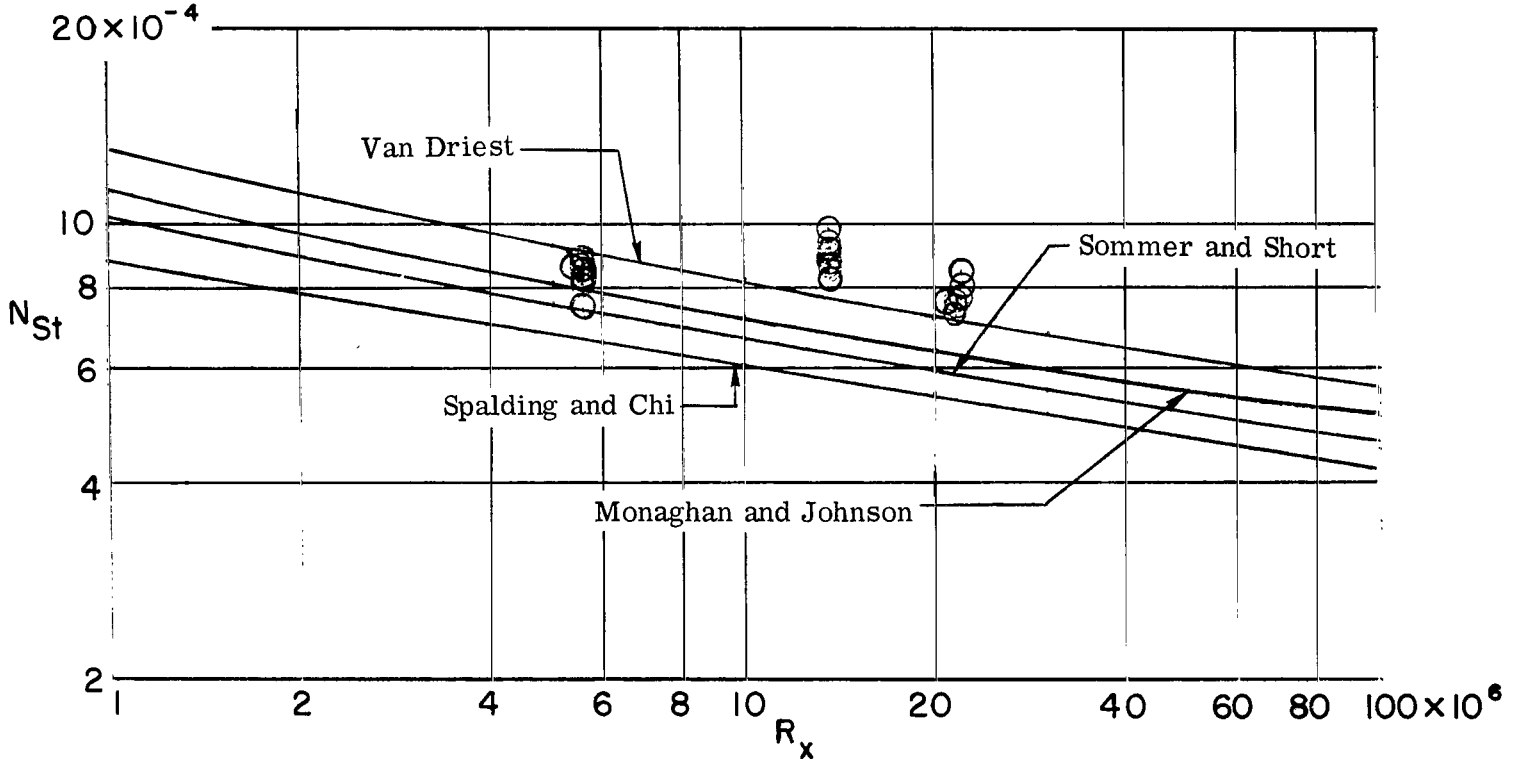

(a) $T_w/T_{aw} = 0.44$.

Figure 22.- Variation of Stanton number with effective Reynolds number.

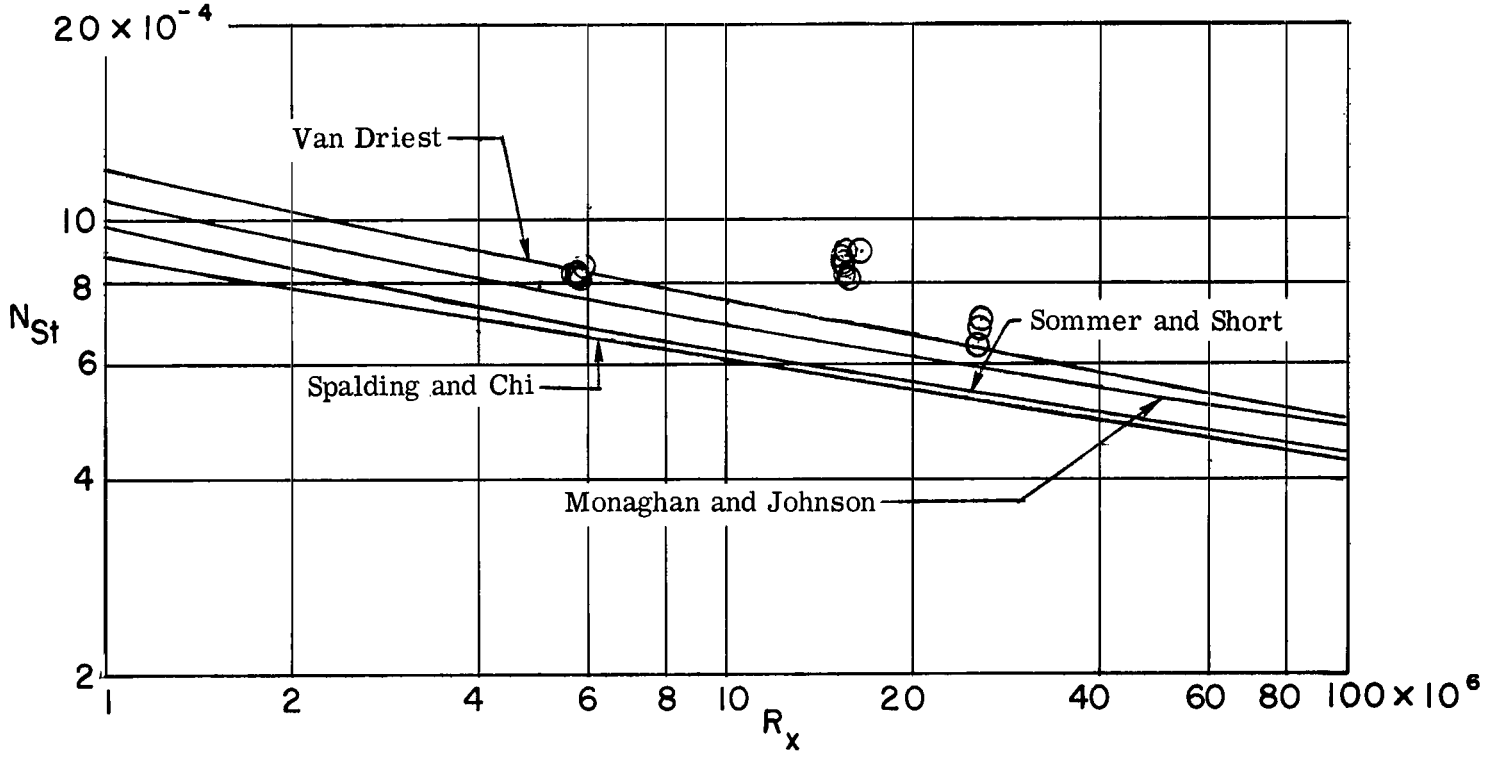

(b) $T_w/T_{aw} = 0.50$.

Figure 22.- Concluded.

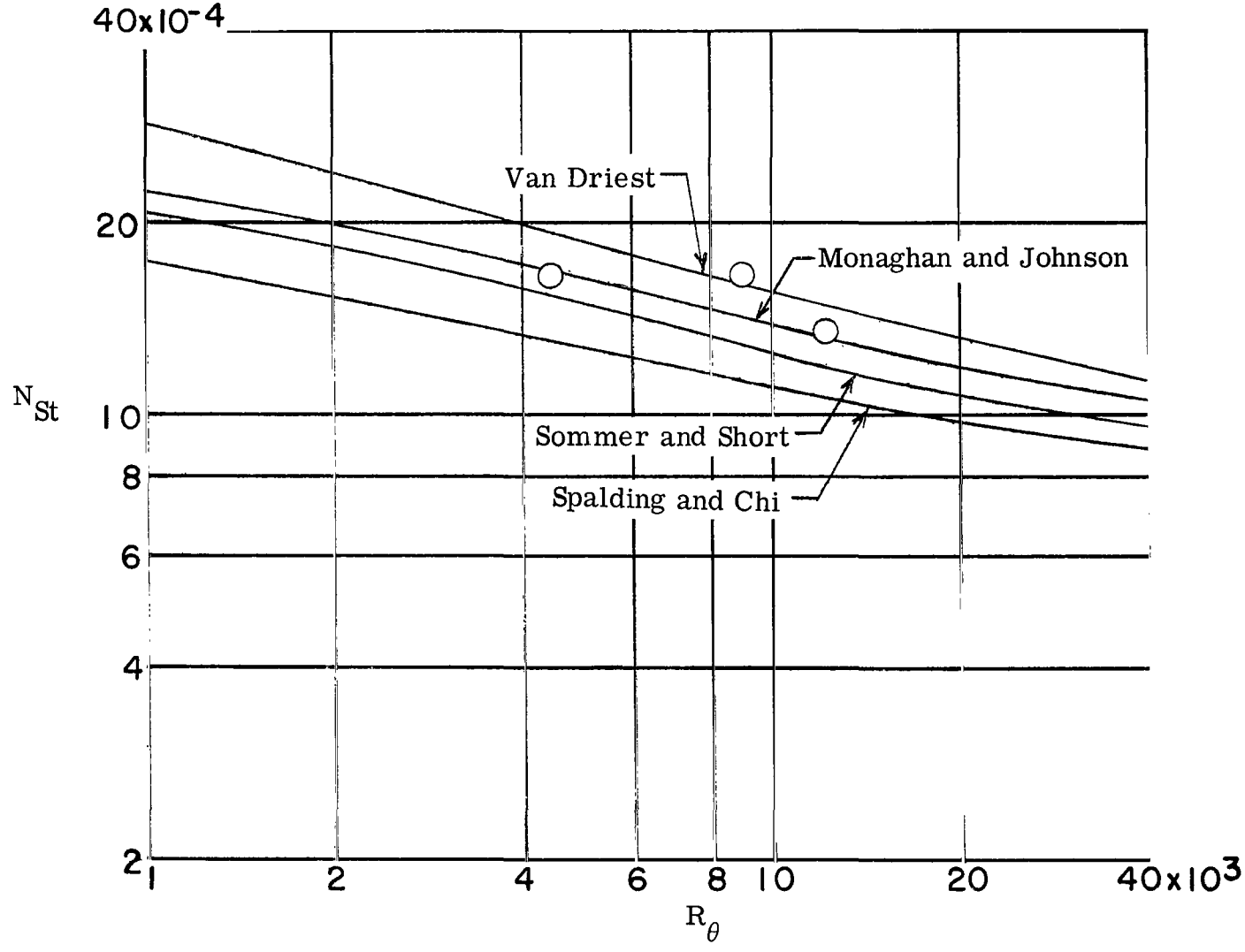

(a) $T_w/T_{aw} = 0.44$.

Figure 23.- Variation of Stanton number with Reynolds number based on momentum thickness.

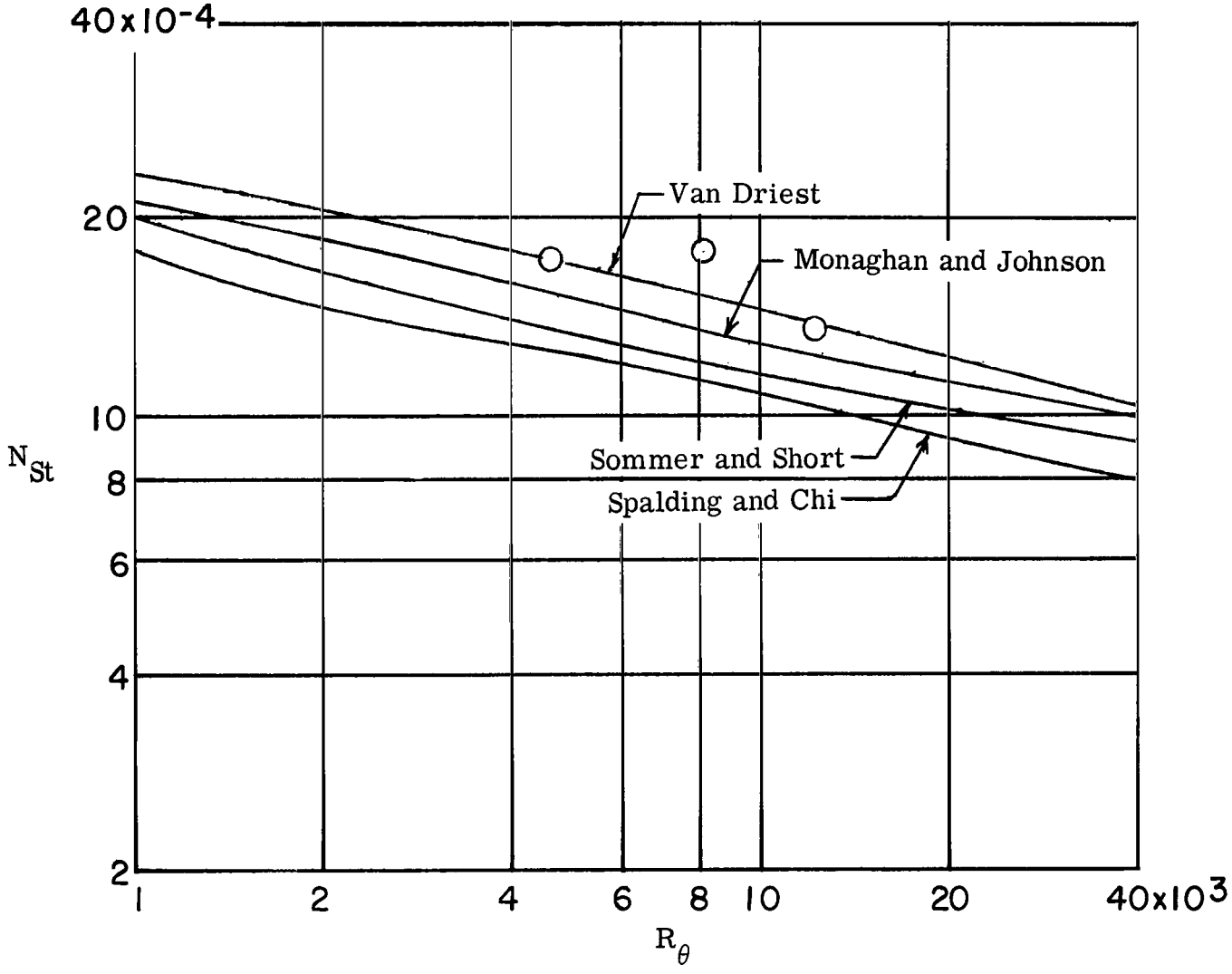

(b) $T_w/T_{aw} = 0.50$.

Figure 23.- Concluded.

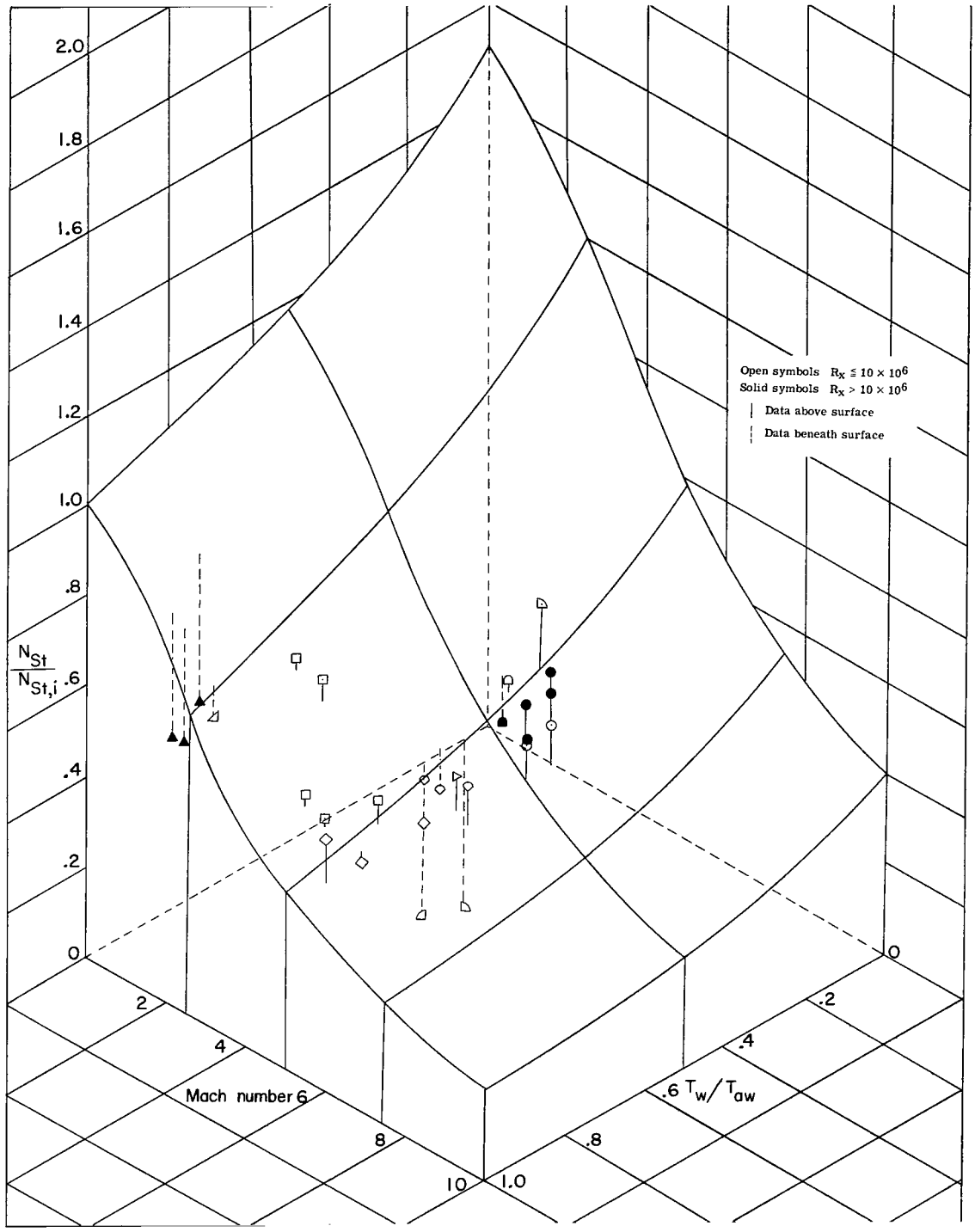

Figure 24.- Variation of experimental Stanton number with Mach number and wall-temperature ratios at various Reynolds numbers. Surface as determined from Sommer and Short T' theory used in conjunction with the Colburn form of Reynolds analogy for $R_x = 10 \times 10^6$.

KEY FOR FIGURE 24

Author	Mach number	T_w/T_{aw}	Reynolds number
○ Present data	6.00	0.44 to 0.50	3.2×10^6 to 23.5×10^6
□ Tendeland (ref. 24)	3.00 to 5.04	0.75 to 0.87	3.5×10^6 to 5.7×10^6
△ Maloney (ref. 22)	1.38 to 2.00	0.85 to 0.96	68.0×10^6 to 75.0×10^6
◇ Winkler and Cha (ref. 2)	5.12 to 5.29	0.66 to 0.92	3.0×10^6 to 4.7×10^6
⌂ Rumsey and Lee (ref. 25)	4.78 to 4.89	0.42 to 0.44	8.4×10^6 to 20.4×10^6
◇ Holloway and Sterrett (ref. 26)	4.89 to 6.00	0.60 to 0.64	3.4×10^6 to 8.8×10^6
◿ Slack (ref. 27)	2.40	0.93	1.2×10^6
▷ Neal (ref. 21)	6.80	0.80	4.8×10^6
◺ Brinich and Diaconis (ref. 19)	4.95	0.35 to 0.93	9.6×10^6

"The aeronautical and space activities of the United States shall be conducted so as to contribute . . . to the expansion of human knowledge of phenomena in the atmosphere and space. The Administration shall provide for the widest practicable and appropriate dissemination of information concerning its activities and the results thereof."

—NATIONAL AERONAUTICS AND SPACE ACT OF 1958

NASA SCIENTIFIC AND TECHNICAL PUBLICATIONS

TECHNICAL REPORTS: Scientific and technical information considered important, complete, and a lasting contribution to existing knowledge.

TECHNICAL NOTES: Information less broad in scope but nevertheless of importance as a contribution to existing knowledge.

TECHNICAL MEMORANDUMS: Information receiving limited distribution because of preliminary data, security classification, or other reasons.

CONTRACTOR REPORTS: Technical information generated in connection with a NASA contract or grant and released under NASA auspices.

TECHNICAL TRANSLATIONS: Information published in a foreign language considered to merit NASA distribution in English.

TECHNICAL REPRINTS: Information derived from NASA activities and initially published in the form of journal articles.

SPECIAL PUBLICATIONS: Information derived from or of value to NASA activities but not necessarily reporting the results of individual NASA-programmed scientific efforts. Publications include conference proceedings, monographs, data compilations, handbooks, sourcebooks, and special bibliographies.

Details on the availability of these publications may be obtained from:

SCIENTIFIC AND TECHNICAL INFORMATION DIVISION

NATIONAL AERONAUTICS AND SPACE ADMINISTRATION

Washington, D.C. 20546